UiT
THE ARCTIC
UNIVERSITY
OF NORWAY

Department of Physics and Technology

Geothermal Energy and District Heating in Ny-Ålesund, Svalbard

—

Julianne Iversen

Master's Thesis in Energy, Climate and Environment EOM-3901
December 2013

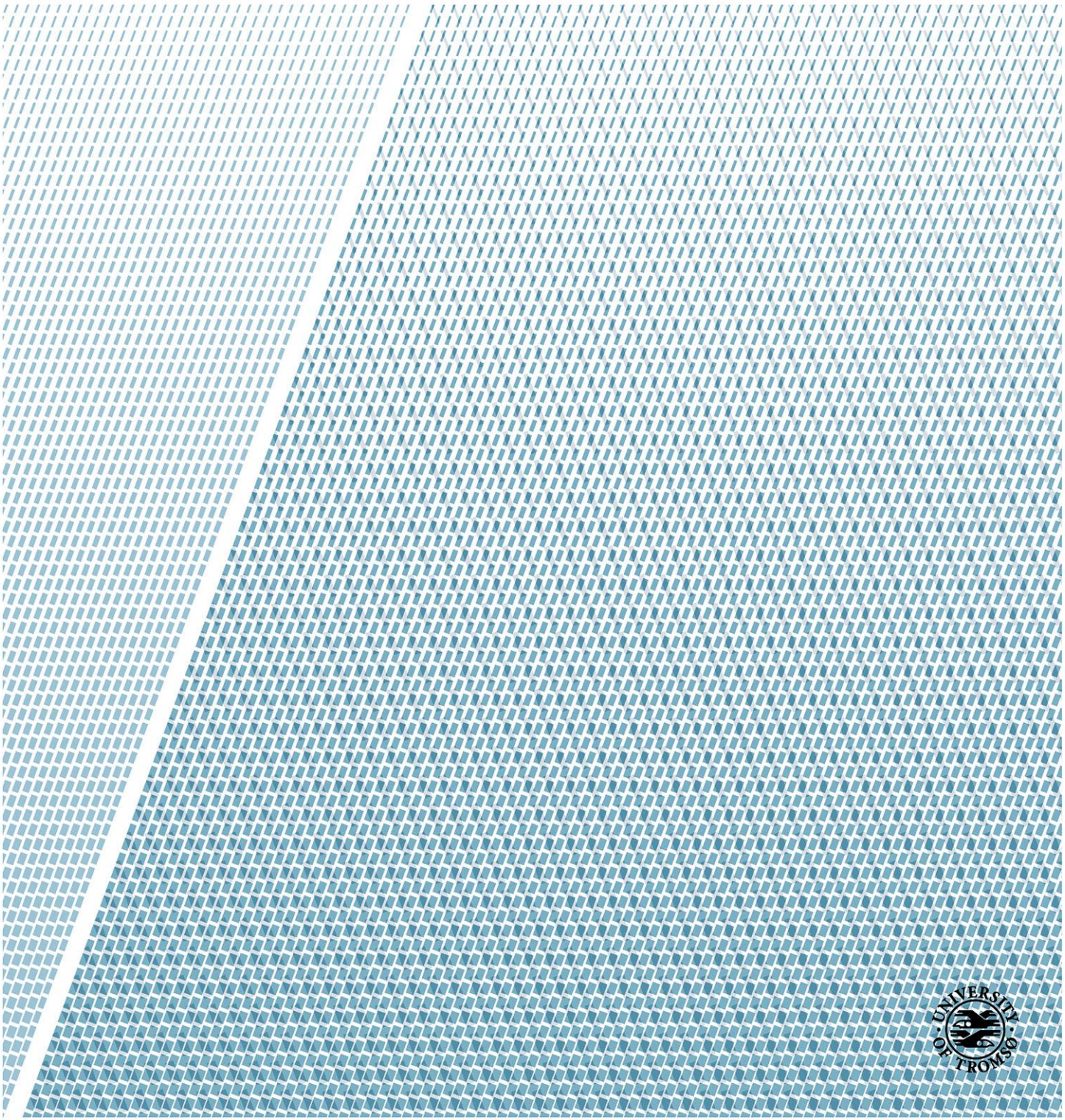

Abstract

This thesis presents the possibilities for using shallow geothermal energy for heating purposes in Ny-Ålesund. The current energy supply in Ny-Ålesund is a diesel generator, which does not comply with the Norwegian government and Ny-Ålesund Science Managers Committee's common goal to maintain the natural environment in Ny-Ålesund. Ny-Ålesund has a potential for replacing the heat from the current diesel based energy source with geothermal energy. Geothermal energy is considered to have low impact on the environment, and is therefore a good alternative to make Ny-Ålesund renewable.

Ny-Ålesund is found suitable for the use of shallow geothermal energy. Considered factors are geology, the geothermal gradient, the groundwater flow and the permafrost depth the area. A geothermal system can be included in the existing district heating system, and replace the heat produced by the diesel generator.

A model containing the geological and physical properties in Ny-Ålesund is created using COMSOL Multiphysics. Simulations of a geothermal system with a 100 meter deep pipe, show that approximately 50 such systems are needed to cover Ny-Ålesund's heating demand. The simulations also show how a geothermal system will influence the temperature distribution around the geothermal pipe, how the geothermal system influences the permafrost depth, and how the groundwater flow effects the ground temperature.

Acknowledgements

First, I would like to thank my supervisor, Yngve Birkelund. I am grateful for all the meetings, advices and support you have given me. The result would not have been the same without your help.

Kirsti Midttømme, thank you for answering my questions and for inviting me to GeoEnergy 2013 in Bergen. The conference was inspiring and helped a lot on my motivation for working with this project.

Krister Leonart Haugen, thank you for helping me when the simulations in COMSOL Multiphysics did not work. Without your help, the simulations would probably take more effort to complete.

Thank you Kine for both the short and long brakes during the studies. The last five years would not have been the same without you. Thanks to Tarjei and all my other fellow students on 'brakka' for the quizzes and for all the good discussions in the lunch breaks.

Beloved Tor, thank you for always being there and always believing in me. Your encouragement and positivity have been more important than anything else.

Julianne Iversen, December 13, 2013

Contents

List of Figures

List of Tables

Chapter 1

Introduction

The current energy supply in Ny-Ålesund is a diesel generator. The Norwegian government and Ny-Ålesund Science Managers Committee (NySMAC) have a goal that the environment in Ny-Ålesund should be pristine, and that the human impact on the environment should be kept to a minimum. The diesel generator has a negative impact on the environment, as it produces air pollution. This is not only negative from an environmental point of view, but there is also ongoing research done by the Norwegian Institute for Air Research on The Zeppelin Observatory, in the vicinity. Measurements from this research station acts as a basis for the study of trends and global atmospheric changes. It is therefore desirable to replace the diesel generator with a renewable energy source [Ore and Øiseth, 2011, Sander et al., 2006, Jørgensen and Bugge, 2009]. Geothermal energy is considered to have low impact on the environment compared to other energy resources [Kristmannsdóttir and Ármannsson, 2003, Rybach, 2003]. Geothermal energy is therefore a good alternative to make Ny-Ålesund renewable.

Geothermal energy is thermal energy extracted from the heat of the earth's interior [Huenges and Ledru, 2011, Glassley, 2010]. In contrast of other renewable energy sources, geothermal energy is independent on external factors, like weather. Consequently, geothermal energy is a stable and reliable energy source.

Geothermal systems are often classified as high enthalpy or low enthalpy systems, based on the temperature of the geothermal fluid that is extracted from the ground [Barbier, 2002, Banks, 2012]. The geothermal fluid are used for different purposes depending on the temperature of the geothermal fluid [Lindal, 1973]. In general, high enthalpy systems are deep geothermal systems that produces electricity [Barbier, 2002, Huenges and Ledru, 2011], and low enthalpy systems are shallow geothermal systems that are used for

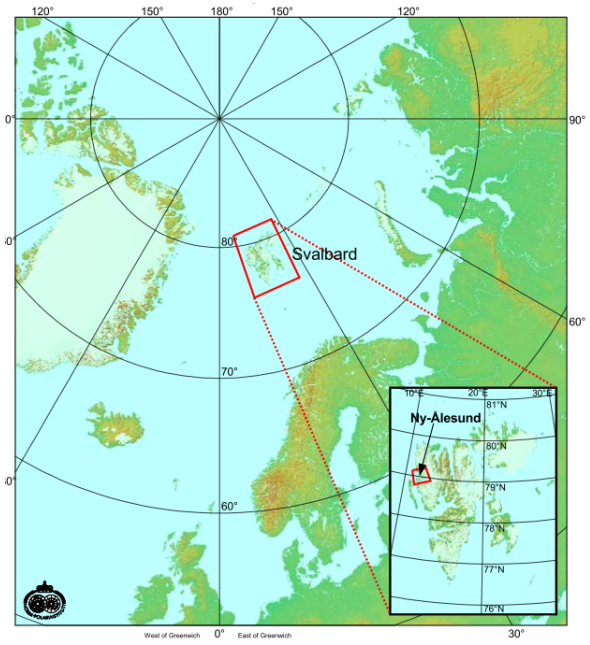

Figure 1.1: *Map showing the location of Ny-Ålesund [Shears* et al.*, 1998]*

heating purposes [Sanner et al., 2011b, Sanner et al., 2011a]. It is normal to use a ground source heat pump to increase the temperature of the geothermal fluid in a shallow geothermal system [Huttrer, 1997, Lund et al., 2004, Omer, 2008].

In Europe, the current installed capacity of geothermal power generation is about $1850MW_{el}$, while the installed capacity of geothermal heating is about $8000MW_{th}$ [Antics et al., 2013]. Shallow geothermal energy has a long history in Norway, and the potential for use of geothermal energy are huge [Ramstad, 2011]. Two of the largest borehole based ground source heat pumps systems in Europe are located in Norway, and 26 000 shallow geothermal systems using a ground source heat pump exists in Norway [Midttømme et al., 2008]. This makes Norway one of the leading countries in increase in geothermal energy use and installed capacity per inhabitant [Midttømme et al., 2010, Lund et al., 2011].

Ny-Ålesund, $78°55'N, 11°56'E$, is one of the northernmost settlements in the world. Figure 1.1 shows that Ny-Ålesund is located on the north-west coast of Spitsbergen, which is the largest island of Svalbard. Most of the settlement of Ny-Ålesund was build by the Kings Bay Kull Company A/S. In 1917 they started mining for coal in the area around Ny-Ålesund. The mining stopped in 1962 after a disaster in one of the mines. Since 1965, Ny-Ålesund has been a multinational research station, where the main re-

search activity has been arctic and climate research. The research activity here is coordinated by the NySMAC. The population of Ny-Ålesund is around 30 in winter and 150 in summer, all connected to the research activity [Shears et al., 1998]. In 2012, there was 12 211 research days, and in total, there was 24 963 overnight stays including researchers, visitors and staff [Øiseth, 2012]. The main goal is to develop Ny-Ålesund as the leading international research and monitoring station in the Arctic.

The main focus for this thesis is to investigate the possibilities for using shallow geothermal energy for heating purposes in Ny-Ålesund. A geothermal system can be included in the existing district heating system, and replace the heat produced by the diesel generator. The geology [Hjelle et al., 1999, Elvevold et al., 2007] and the groundwater conditions [Haldorsen and Lautitzen, 1993, Haldorsen et al., 1996, Booij et al., 1998] in Ny-Ålesund are studied to find out if the area is suitable for a geothermal system. A challenge for installing a geothermal system in Ny-Ålesund is the cold climate. Permafrost dominates the subsurface in the area around Ny-Ålesund [Liestøl, 1980, Humlum et al., 2003, Sollid et al., 2000, Isaksen et al., 2001]. Ground source heat pumps working in cold climate is also essential to lift the temperature of the geothermal fluid to a desired level [Guoyuan et al., 2003, Bakirci, 2010].

A simulation of a shallow geothermal system, using COMSOL Multiphysics, has been created to give an indication of the amount of heat such a system can deliver. The simulations shows the changes in the temperature distribution in the ground when installing a geothermal system, and the influence from the groundwater flow on the geothermal system. If a geothermal system should be installed in Ny-Ålesund, this results can give an indication on the required size of the geothermal system and also on the required properties of the heat pump.

1.1 Structure of the thesis

This thesis is divided into 5 chapters.

Chapter 2 includes an introduction to geothermal energy, and is divided into three parts. The first part explains the physical aspects of geothermal energy, and includes thermodynamic concepts, fluid mechanics, heat sources and heat transport. The next part describes geological aspects of geothermal energy. The last part of this chapter includes technology aspects of geothermal energy. Here, the different types of geothermal system are described as well as heat pump technology. Chapter 2 can be used independent as an introduction to geothermal energy.

Chapter 3 describes Ny-Ålesund in terms of geology, climate and groundwater conditions. The energy production and energy consumption are also described here.

Chapter 4 contains a discussion of the alternatives for making the energy in Ny-Ålesund renewable. The discussion is supported by a model and several simulations done in COMSOL Multiphysics. The results of the simulations, and the parameters of the model are also covered in this chapter. Chapter 3 and Chapter 4 are the most important chapters in this thesis.

The conclusion and proposals for future work are presented in Chapter 5.

Chapter 2

Background for Geothermal Energy

2.1 Physics

2.1.1 General thermodynamic concepts

Thermodynamic concepts deals with three closely related terms; temperature, heat and energy. Energy is one of the most fundamental concepts in physics. Energy can never form or disappear, it can only be converted from one form to another. The first law of thermodynamics states that the energy in an isolated system always is conserved. The SI-unit for energy is Joule [J], and it is defined as

$$1J = kg\frac{m^2}{s^2} \tag{2.1}$$

Heat is defined as the spontaneous flow of energy caused by a temperature difference between two objects. In thermodynamics, the term temperature is a measurement of a materials tendency to spontaneously give up energy [Schroeder, 2000].

The first law of thermodynamics

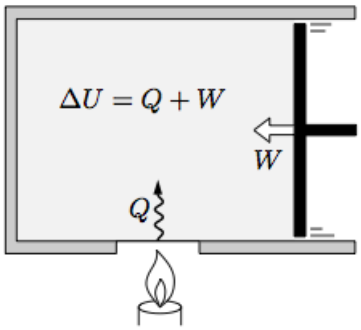

Figure 2.1: *Visual representation of the first law of thermodynamics [Schroeder, 2000]*

The first law of thermodynamics states that [Schroeder, 2000]

$$\Delta U = Q + W \tag{2.2}$$

where ΔU [J] is the change in the internal energy Q [J] is the heat added/-subtracted to the system and W [J] is the work done on or by the system.

The change in the internal energy of the system is the sum of the work done on, or done by, the system and the heat added, or subtracted, by the system. The terms in the first law of thermodynamics can be negative if heat or energy leaves the system. Figure 2.1 shows a visual representation of the first law of thermodynamics. In this figure, the candle light adds heat to the system and the piston performs work on the system. The first law of thermodynamics is just a reformulation of the law of conservation of energy.

The second law of thermodynamics

The second law of thermodynamics states that any large system will in equilibrium be at the state that is most probable, or more precise, the state with the highest multiplicity.

The microstate of a system specifies the state of each particle in the system, while the macrostate of a system specifies the different states the particles have available. The multiplicity of a macrostate is the number of microstates corresponding to that macrostate. The state with the highest multiplicity have the highest probability to occur.

The second law of thermodynamics also tells that heat will flow from a hot part of a material to a cold part of a material, since the hot state have higher multiplicity than the cold. The second law of thermodynamics is a statistical law, and therefore there is a probability that heat will flow from cold to hot, but this probability is tremendously small.

Entropy

The definition of entropy, S [J/K], is as follows [Schroeder, 2000]

$$S \equiv k \ln \Omega \tag{2.3}$$

where k = $1.381 \times 10^{-23} J/K$ is the Boltzmann's constant and Ω is the multiplicity.

The multiplicity of a system is the number of ways of arranging the particles in the system. If the multiplicity of a system increases, this means that the number of available states increases as well as the disorder of the system. Since the multiplicity is the only depending factor in the definition of entropy, one can think of entropy as a measure of the disorder in a material.

A example that illustrates the term entropy is a deck of cards. If the cards is shuffled, the disorder is larger than if the deck is sorted. The number of possible arrangements is larger when the deck is shuffled and therefore the entropy is larger.

Enthalpy

The definition of enthalpy, H [J], is as follows [Schroeder, 2000]

$$H \equiv U + PV \tag{2.4}$$

where U is the internal energy [J], V is volume [m^3] and P is pressure [Pa].

Enthalpy is a measure of the energy in a thermodynamic system. Enthalpy is the energy needed to create a system in addition the energy needed to make room for the system in an environment with constant pressure. Enthalpy can also be considered as the thermal potential of a system since the definition of enthalpy consider both the temperature and the pressure.

Heat capacity and latent heat

The heat capacity, C [JK^{-1}], of an object describes how the temperature ΔT [K] to the object rises if heat Q [J] flows into the object. The heat

capacity of an object is given as [Schroeder, 2000]

$$C \equiv \frac{Q}{\Delta T} \tag{2.5}$$

The specific heat capacity, c $[Jkg^{-1}K^{-1}]$, of an object is defined as the heat capacity C per unit mass m [kg], and can be expressed as [Schroeder, 2000]

$$c = \frac{C}{m} \tag{2.6}$$

The heat capacity of an object can be measured and given in two different ways. If the first law of thermodynamics, Equation 2.2, is included in the expression for heat capacity, Equation 2.5, one get

$$C = \frac{Q}{\Delta T} = \frac{\Delta U - W}{\Delta T} \tag{2.7}$$

If no work is done on the system and its volume is held constant, one can measure the heat capacity at constant pressure. In the example in Figure 2.1 the piston is not moving, and therefore V is constant. The heat capacity at constant pressure is expressed as

$$C_V = \left(\frac{\Delta U}{\Delta T}\right)_V = \left(\frac{\delta U}{\delta T}\right)_V \tag{2.8}$$

If an object is heated, the volume tend to increase. In this case the system does work on the surroundings, since W is negative. C is then larger than C_V, and additional heat is needed to compensate for the energy lost as work.

The heat capacity can also be measured when the pressure is held constant. If the work added to the system is compression work, $W = -P\Delta V$, the heat capacity at constant pressure can be written as

$$C_P = \left(\frac{\Delta U - (-P\Delta V)}{\Delta T}\right)_P = \left(\frac{\delta U}{\delta T}\right)_P + P\left(\frac{\delta V}{\delta T}\right)_P \tag{2.9}$$

Latent heat, L $[Jkg^{-1}]$, is the amount of heat required to make a material undergo a phase transformation. The latent heat can be expressed as [Schroeder, 2000]

$$L \equiv \frac{Q}{m} \tag{2.10}$$

where Q [J] is the heat required for a phase transformation of a mass m [kg].

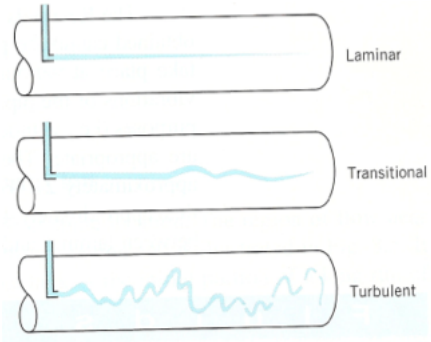

Figure 2.2: *Laminar, transitional and turbulent flow in a pipe [Munson* et al.*, 2006]*

2.1.2 Fluid Mechanics

Fluid flow in a pipe

The flow of a fluid can be described as either laminar, transitional or turbulent [Munson et al., 2006]. The characteristics of the fluid flow are illustrated in Figure 2.2.

Reynolds number is an important variable in the study of a viscous fluid through pipes. It is often used as a criterion to distinguish between laminar and turbulent flow through a pipe. Reynolds number is defined as [Banks, 2012]

$$Re = \frac{2r\rho F}{\mu A} \tag{2.11}$$

where F $[m^3 s^{-1}]$ is the flow rate, μ $[kgm^{-1}s^{-1}]$ is dynamic viscosity and ρ $[kgm^{-3}]$ is the density of the fluid. A $[m^2]$ is the cross section of the pipe and r [m] is hydraulic radius.

If the Reynolds number is less than 2300, the fluid flow is classified as laminar. The fluid flow is classified as transient turbulent if the Reynolds number is between 2300 and 9000. A fluid flow with Reynolds number higher than 9000 is classified as fully turbulent [Banks, 2012].

Darcy's law

Darcy's law is analogous to Fourier's law, Equation 2.19, which describes heat conduction. Darcy's law describes how a fluid flow through a porous media. Darcy's law is dependent on the term *head* (h), which combines elevation (z) and pressure (p). A fluid will flow in the direction of lower elevation

as well as lower pressure. The definition of head is given by [Banks, 2012]

$$h = z + \frac{p}{\rho_w g} \tag{2.12}$$

where ρ_w is the water density and g is the acceleration due to gravity. This definitions tells that groundwater always will flow in the direction of lower head. The head is also a measure of the potential energy of the groundwater. The groundwater will always flow in the direction according to Darcy's law.

Darcy's law is given as [Banks, 2012]

$$Z = -KA\frac{dh}{dx} \tag{2.13}$$

where Z $[m^3 s^{-1}]$ is the flow of water, K $[ms^{-1}]$ is the permeability of the porous media, A $[m^2]$ is the cross section and x [m] is the distance in the direction of the head. $\frac{dh}{dx}$ is the head gradient.

2.1.3 Heat sources

Heat from the sun

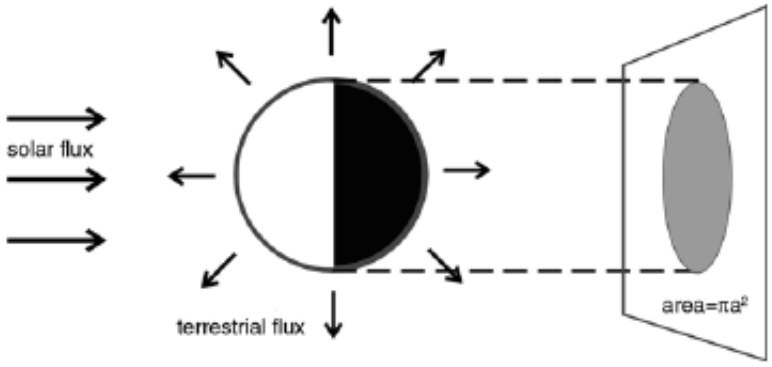

Figure 2.3: *Geometry and assumptions for the calculations of the energy balance of the earth [Marshall and Plumb, 2007].*

The most important heat source for the earth is the heat flow from the sun. The solar energy is not evenly distributed on the earth's surface, it depends on the latitude. The highest annual solar radiation is on equator, where the radiation is measured to be over $2000 kWhm^{-2}$ per year, while in northern Europe the radiation can be less than $1000 kWhm^{-2}$ [Boyle, 2004]. The incoming solar radiation is also depends on the seasons, because of the tilting

of the earth. In June, the north pole is tilted towards the sun, and therefore the solar radiation is be higher on the northern hemisphere. In December, the north pole is tilted away from the sun, and the solar radiation here is less. The opposite case will happen on the southern hemisphere, where the solar radiation will be higher in December and less in June.

The amount of energy emitted from the sun is $Q = 3.87 \times 10^{26} W$ [Marshall and Plumb, 2007]. The solar constant describes the average heat flux that the earth receives from the sun, measured on an imaginary plane perpendicular to the sun, just outside the earth's atmosphere [Banks, 2012]. The solar constant is defined as [Marshall and Plumb, 2007]

$$S_0 = Q/4\pi r^2 \tag{2.14}$$

where $r = 150 \times 10^9 m$ is the average distance between the sun and the earth. This gives a solar constant of $S_0 = 1368 W/m^2$. The solar constant is the heat flux from the sun on the average distance from the earth to the sun.

Not all of the incoming solar radiation is absorbed by the earth, some of is reflected back into space. The solar constant, S_0, does not consider that the earth reflects the sunlight, and is therefore a maximal theoretical value. Albedo is defined as a percentage which tells how much of the incoming sunlight that is reflected by the earth's surface [Houghton, 2009]. On average, 30 percent of the incoming solar radiation is reflected back to space [Houghton, 2009]. This is known as the planetary albedo.

From the illustration in Figure 2.3, the incoming solar radiation on the earth's cross section can be calculated as $S_0 \pi R^2$, where $R = 6.37 \times 10^6 m$ km is the average radius of the earth. In the calculations of the energy balance of the earth, it is assumed that the earth receives solar energy over a disk with radius equal to the earth's radius. It is also assumed that the earth's radiation is isotropic. Figure 2.3 illustrates these assumptions.

The solar radiation that is absorbed by the earth can then be calculated as [Marshall and Plumb, 2007]

$$\begin{aligned} &\text{Solar radiation absorbed by the earth} \\ &\quad = (1 - \alpha_p) S_0 \pi R^2 = 1.22 \times 10^{17} W \end{aligned} \tag{2.15}$$

where $\alpha_p = 0.3$ is the planetary albedo [Houghton, 2009].

The earth also emits energy, in the same rate as the absorption of energy from the sun. This is further discussed in Section 2.1.4.

Heat from the earth's interior

The interior of the earth has a temperature between $3000°C$ and $5000°C$ [Omer, 2008]. Radioactive decay in the earth's core is one of the main reasons that the core is still hot. These radioactive elements was formed during the formation of the earth, and they are still radioactive because of their long half-life. The gravitational force acting on the earth's core is also an important reason that the core has high temperature.

The second law of thermodynamics, discussed in Section 2.1.1, states that heat tends to go from high to low temperature, and this means that the earth's core constantly radiates a heat flux towards the surface. The average heat flux from the earth's interior to the earth's surface is $0.087 W m^{-2}$ [Pollack et al., 1993]. The variations of the heat flux on the earth is large, mostly depending on the tectonic regime in the area. Geology and tectonics are described in Section 2.2.

Heat from radioactive decay in the crust

General about radioactive decay For a neutral atom, the number of protons and electrons are the same. The sum of the number of protons and neutrons in the core of an atom is called nucleons. The nucleon number is defined as $A = Z + N$ where Z is the number of protons and N is the number of neutrons. An element always has the same number of protons in the core, but the number of neutrons can vary. An atom core with Z protons and A nucleons are denoted as

$$^{A}_{Z}X$$

where X is the chemical symbol. The different variants of the element are called isotrops. Isotrops can be stable, but most of the isotrops are unstable. An unstable isotrop emits ionizating decay and this is called radioactivity. The ionizating decay is a result of the atom having excess energy. Radioactive decay is divided into three different types of radiation; alpha-, beta- and gamma decay.

Alpha decay is the emission of a helium atom while beta decay is the emission of an electron. Gamma decay is decay of high energy photons. The core of an atom can be in different energy states, and after alpha or beta decay, the atom core is in an excited state. An excited atom is in a higher energy state than its ground state. When the atom returns to the ground state, the core emits a photon. This is called gamma decay.

The energy from a nuclear decay is given by Einstein's equation

$$E = mc^2 \tag{2.16}$$

where E is the energy released, m is the mass and $c = 3 \times 10^8 m/s$ is the speed of light.

Nucleus is the collection of protons and neutrons in the core of an atom. The radioactive decay law tells us how many radioactive nuclei that are present, and is defined by the following equation [Giancoli, 2008]

$$N = N_0 e^{-\lambda t} \tag{2.17}$$

where N is the number of radioactive nuclei present, N_0 is the number of nuclei present at time t = 0 and λ is the decay constant which describes the rate of decay of an isotope.

The half-life of a radioactive atom is the time it takes before half of the atom core in a radioactive material is transformed into new atom cores. The rate of decay is normally given in half-life instead of the decay constant above. From the decay law, Equation 2.17, the half-life can be calculated when $t = \frac{T}{2}$

$$\begin{aligned} \tfrac{N_0}{2} &= N_0 e^{-\lambda T_{1/2}} \\ e^{-\lambda T_{1/2}} &= 2 \\ T_{1/2} &= \tfrac{\ln 2}{\lambda} \end{aligned} \tag{2.18}$$

Radioactivity in the crust There still exists radioactive materials in the earth's crust from the creation of the earth 4.5 billion years ago. These materials have long half-life. As described above, radioactive isotopes creates heat, and therefore, these isotopes are a heat source in the earth's crust. The main radioactive isotopes that contributes to the creation of heat in the crust are uranium ($^{235}_{92}U$ and $^{238}_{92}U$), thorium ($^{232}_{90}Th$) and potassium ($^{40}_{19}K$) [Barbier, 2002]. $^{238}_{92}U$ is the most common isotope of uranium, and this isotope has a half-life of 4.468×10^9 years. Figure 2.4 shows the decay series for $^{238}_{92}U$.

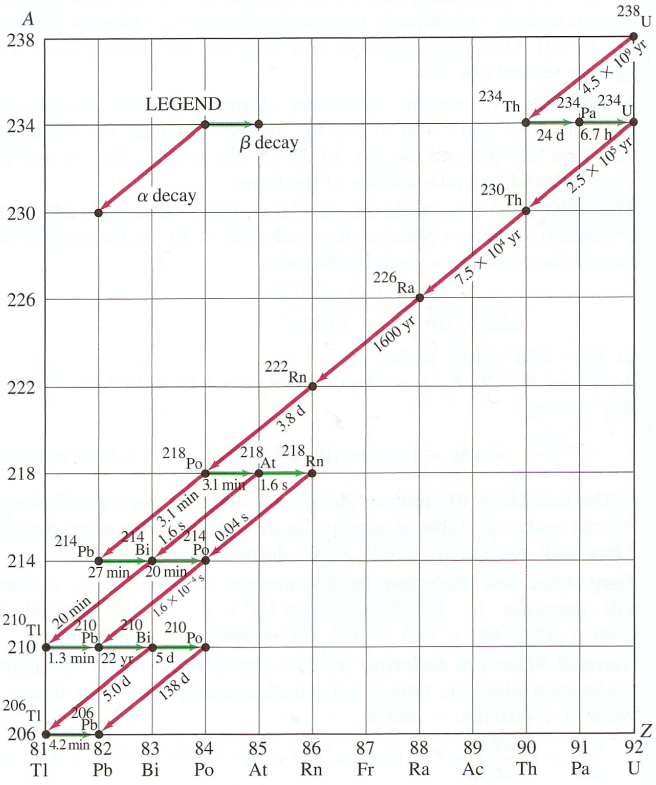

Figure 2.4: *Decay series for* $^{238}_{92}U$ *[Giancoli, 2008]*

2.1.4 Heat transport

There are three ways that heat is transported from a heat source; by conduction, by convection and by radiation.

Conduction

Conduction is the transfer of heat between two materials. These materials can be solid, liquid or gas. The conduction of heat is caused by the temperature difference between the two materials, and is a result of molecular interaction.

The fast moving molecules in a warm part of the material, give away some of their energy when they are in contact with slow moving molecules in a cold part of the material. This is the way heat is transferred between two materials with different temperatures. All materials do not conduct heat at

the same speed. The thermal conductivity (λ $[Wm^{-1}K^{-1}]$) describes how well a material can conducts heat.

Fourier's law tells us how much heat is conducted (Q $[Js^{-1}]$) through a given material [Banks, 2012]. The terms in Fourier's law are illustrated in Figure 2.5.

$$Q = -\lambda A \frac{dT}{dx} \tag{2.19}$$

Here, A $[m^2]$ is the cross section area of the block of consideration, x [m] is the distance coordinate in the direction of decreasing temperature and $\frac{dT}{dx}$ $[Km^{-1}]$ is the temperature gradient.

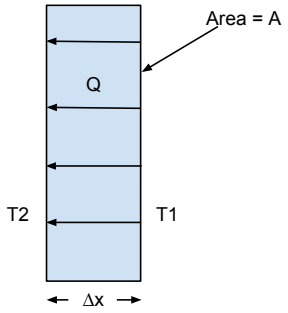

Figure 2.5: *Visual representation of the terms in Fourier's law. [Schroeder, 2000]*

Within the earth, heat is transferred between the hot core and the colder mantel by conduction. This results in a geothermal gradient. The geothermal gradient is a measure of how fast the temperature within the earth rises with depth. The average geothermal gradient on the earth is $30°C/km$ [Barbier, 2002]. The temperature distribution within the earth is complex since the geothermal gradient also depends on the mantle convection. The geothermal gradient varies from location to location, depending on the geology. This will be further discussed in Section 2.2.4.

Convection

Convection is the main mechanism for heat transport in a fluid [Schroeder, 2000]. Heat transfer caused by the motion of a fluid is called convection. Convection can not occur in a solid, since the motion of molecules in a solid is limited. The rate of which fluid is transferred in a moving stream of fluid is described by Newton's law of cooling [Banks, 2012].

$$q^* = \bar{h} \times (\theta_{body} - \theta_{fluid}) \tag{2.20}$$

Here, q^* $[Wm^{-2}]$ is the heat transfer from the fluid to the body. The coefficient of heat transfer, $\bar{h}$ $[Wm^{-2}K^{-1}]$, is dependent on the physical characteristics of the fluid and the body. θ_{body} [K] is the temperature of the body and θ_{fluid} [K] is the temperature of the fluid.

If a fluid is transported by using mechanical energy, for example a water pump, then the motion of heat is called forced convection, or advection [Banks, 2012]. Newton's law of cooling is a good approximation of forced convection and when the temperature difference between the body and the fluid is small.

Convection is also an overturning motion caused by the expansion and contraction when a fluid is heated or cooled. In a gravitational field, when a fluid is heated from below or cooled from above, there will be convection in the fluid. This is called natural convection, and the overturning motion creates a convection cell [Marshall and Plumb, 2007]. In the interior of the earth the mantel is heated by the hot core. The result is a convection motion in the mantel.

Radiation

The solar radiation that is absorbed by the earth was calculated in section Section 2.1.3 to be $1.22 \times 10^{17} W$. The earth also emits energy (q_e $[Wm^{-2}]$), in the same rate as the absorption, to maintain equilibrium. The emitted radiation is described by the Stefan-Boltzmann law [Schroeder, 2000]

$$q_e = \sigma T_e^4 \tag{2.21}$$

where $\sigma = 5.67 \times 10^{-8} Wm^{-2}K^{-4}$ is the Stefan-Boltzmann constant and T_e [K] is the emission temperature of the earth.

The total emitted radiation from the earth can be calculated as

$$Q_e = 4\pi R^2 \sigma T_e^4 \tag{2.22}$$

where Q_e [W] is the total emitted energy and R [m] is the radius of the earth.

When the absorbed radiation from the sun (Equation 2.15) and the emitted radiation from the earth, (Equation 2.22) are in equilibrium, the emission

temperature can be calculated as

$$\begin{aligned} 4\pi R^2 \sigma T_e^4 &= (1-\alpha_p) S_0 \pi R^2 \\ 4\sigma T_e^4 &= (1-\alpha_p) S_0 \\ T_e^4 &= \left[\frac{S_0(1-\alpha_p)}{4\sigma}\right] \\ T_e &= \left[\frac{S_0(1-\alpha_p)}{4\sigma}\right]^{1/4} \\ T_e &= \left[\frac{1368 W m^{-2}(1-0.3)}{4\times 5.67\times 10^{-8} W m^{-2} K^{-4}}\right]^{1/4} \\ T_e &= 255K \end{aligned} \tag{2.23}$$

The emission temperature, $T_e = 255K$, is the temperature the earth needs to emit in order to maintain energy balance, assuming that the average temperature is not decreasing. The global average temperature on the surface is $T_s = 288K$, which is cooler than the emission temperature [Marshall and Plumb, 2007]. The emission temperature are higher mainly because of the radiation observed in the atmosphere and because of the fluid motion within the atmosphere.

2.2 Geology

2.2.1 Structure of the earth

The earth can be divided into three main parts: core, mantel and crust. The structure of the earth is shown in figure Figure 2.6.

The earth's core can be divided into the inner and outer core. The inner core, with a radius of approximate 1220 km, is solid because of the immense pressure inside of the planet. The outer core, with a radius of approximate 2900 km, is liquid.

The mantle is the most volumetric part of the planet. 82 % of the volume of the planet is contained within the mantel [Lutgens et al., 2009]. The solid upper mantel, down to a depth of 660 km, can be separated into the lithosphere and the asthenosphere. The lithosphere is the uppermost part of the mantel. The crust is also contained in the lithosphere. Under continents, the lithosphere is approximate 70 km thick and beneath the sea the lithosphere is about 120 km thick. The lithosphere is divided into several lithospheric plates, as shown in Figure 2.7.

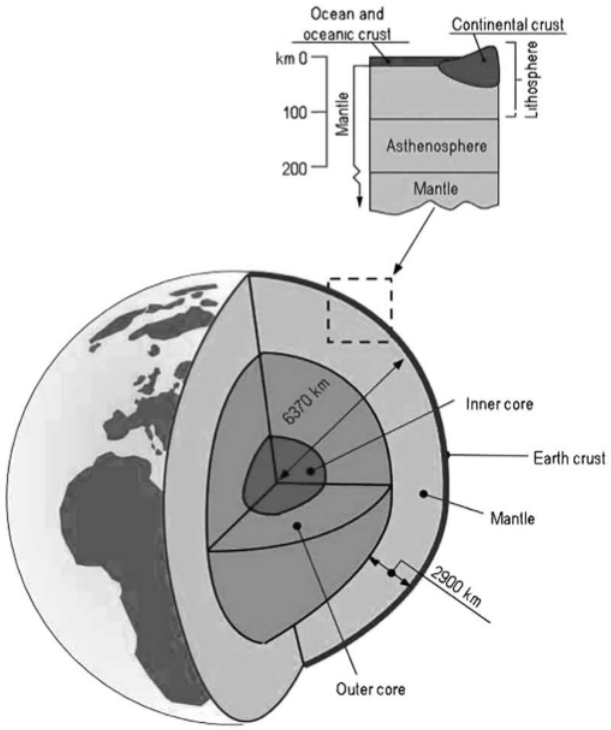

Figure 2.6: *Structure of the earth [Barbier, 2002]*

2.2.2 Tectonics

Alfred Wegener was the first to explain the continental drift [Wegener, 1929]. Wegener believed that a supercontinent, which he called Pangea, once had existed. He believed that the continents had drifted from this supercontinent to their current position. Wagener's idea was radical, but he had several evidences that proved his idea.

The theory of plate tectonics developed in the late 1960s. In contrast to Wegener's theory, where only the continents move, the theory of plate tectonics states that the earth has several lithospheric plates that move. This theory is today accepted by most geologists. The lithospheric plates is shown in Figure 2.7.

Seismic activities such as volcanoes and earthquakes are often found along the boundary between the lithospheric plates.

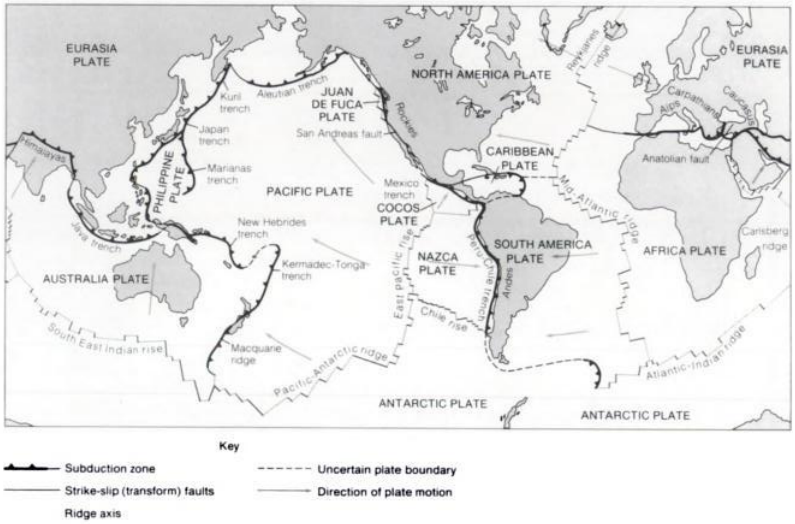

Figure 2.7: *Map that shows the tectonic plates and the different boundaries between them [Schubert* et al.*, 2001]*

There are three main types of margins between the lithospheric plates; divergent, convergent and transform plate margins.

Divergent plate margins

Divergent plate margins is where two lithospheric plates move apart. This results in a upwelling of material from the mantel. If two oceanic plates

move apart, the upwelling mantel material will create new seafloor. Two continental plates can also be located in a divergent plate margin. In a divergent plate margin, new lithosphere is created, and therefore divergent plate margins are also known as constructive plate margins. Figure 2.8 shows two oceanic plates in a divergent plate margin. Iceland is located on the Mid-Atlantic ridge, which is a divergent plate margin between the Eurasian plate and the North American plate.

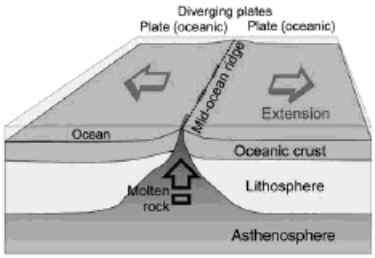

Figure 2.8: *Divergent plate margin [Banks, 2012]*

Convergent plate margins

Convergent plate margins is where two lithospheric plates collide. The oceanic lithospheric plates are lightweight than the continental plates due to their mineralogy composition, and therefore, when a continental plate collides with an oceanic plate in a convergent plate margin, the oceanic plates will descend beneath the continental plate. The oceanic plate will eventually be melted by the mantel, and this will create a continental volcanic arc. Figure 2.9 shows a convergent plate margin where an oceanic plate collides with a continental plate.

If two oceanic plates collide in a convergent plate margin, the lighter oceanic plate will descend beneath the heavier, and create an arc with volcanic islands. Mountain belts are made by convergent plate margins. When two continental plates move towards each other, both continental plates will be pressed upwards and create a mountain belt. As an example, the Himalayas is a result of the Australian-Indian plate colliding in the Eurasian plate. Because of the melting of lithosphere in a convergent plate margin, they are also called destructive plate margins.

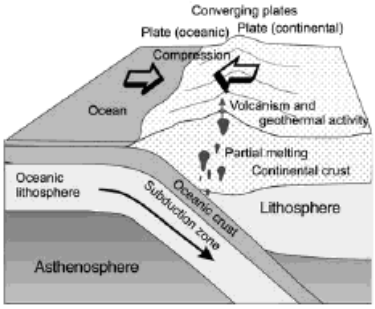

Figure 2.9: *Convergent plate margin [Banks, 2012]*

Transform plate margins

Transform plate margins is also known as conservative plate margins. The reason for this is that no lithosphere is either constructed or destroyed. In a transform plate margin, the two lithospheric plates have movement parallel to each other. A well known example of a transform plate margin is the San Andreas Fault in California, USA.

2.2.3 Geothermal gradient

Geothermal energy is energy that is extracted from the heat of the earth's interior. Not all geothermal systems produce electricity, for example some systems produces hot water for heating purposes. Therefore, geothermal energy is often called an energy saving action and not a renewable energy source.

The geothermal gradient is a measure of how the temperature in the earth's interior increases with depth. The temperature of the upper subsurface is controlled by the air temperature, but deeper than this zone of seasonal temperature fluctuations, the temperature increases with the geothermal gradient. A typical geothermal gradient is $0.01 - 0.03°Cm^{-1}$ [Banks, 2012]. Figure 2.10 shows how the temperature increases with depth with a geothermal gradient of $0.01 - 0.03°Cm^{-1}$. The temperature of the upper subsurface is affected by the annual air temperature down to approximately 10 meters [Banks, 2012]. Note that this geothermal gradient is not typical in areas with volcanic activity or other sources that increases the geothermal gradient. Different reasons for the geothermal gradient to increase are discussed in 2.2.4. The regions with increased geothermal gradient are good locations for geothermal systems.

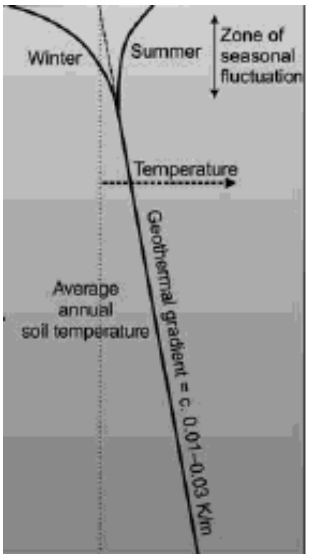

Figure 2.10: *Typical geothermal gradient. The temperature of the upper subsurface are dependent on the annual air temperature. Segment from [Banks, 2012]*

2.2.4 Geology of geothermal regions

Geothermal anomalies due to plate tectonics

As a result of melting of lithosphere in a convergent plate margin, and the upwelling mantel in a divergent plate margin, these areas will have an increased geothermal gradient. In convergent plate margins and divergent plate margins, the average heat flux from the earth's interior through the earth's surface is $0.3Wm^{-2}$ [Boyle, 2004]. The global average heat flux is $0.087Wm^{-2}$ [Pollack et al., 1993]. Because of the increased heat flux and therefore increased geothermal gradient, a geothermal power plant will be desired in the area of a plate margin.

Note that, in contrast to convergent and divergent plate margins, there will not be an increased geothermal gradient in a transform plate margin. Plate margins are discussed in Section 2.2.2.

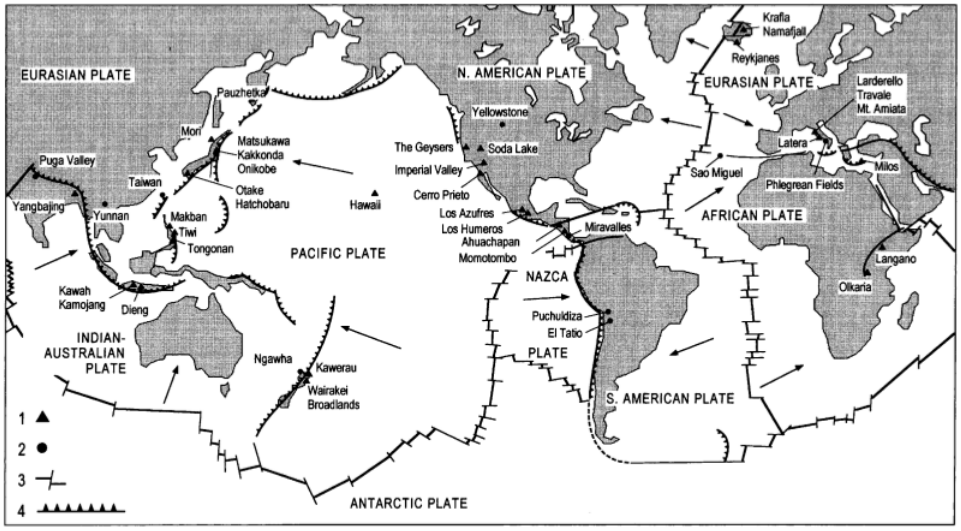

Figure 2.11: *Map that shows the tectonic plates. The figure also includes the current geothermal fields that produce electricity. Legend: 1) Geothermal fields under exploitation, 2) Geothermal fields not exploited, 3) Transform plate margin, 4) Convergent plate margin. [Barbier, 2002]*

Figure 2.11 shows all the plate margins in addition to the current fields that produce electricity. From this figure, one can see that the major geothermal fields that produce electricity are located on the margins between the tectonic plates. Geothermal plants that can produce electricity are normally high temperature, or high enthalpy systems. These systems will be discussed in Section 2.3.4.

There are also increased geothermal gradient in areas around a hot spot. Hot spots are areas where volcanic activity is common. The volcanic activity around a hot spot is caused by upwelling of magma, but this is not caused by a divergent plate margin. The local upwelling of magma is caused by the mantel convection [Lutgens et al., 2009] discussed in Section 2.1.4. A well known hot spot is located on Hawaii. The geothermal gradient in the area of a hot spot is increased, and Figure 2.11 shows that Hawaii is an area that is under exploration to determine if it is suitable for extraction of geothermal energy.

Other geothermal anomalies

Geothermal anomalies can also appear on places other than plate margins.

Thermal conductivity of rocks Fourier's law, Equation 2.19, describes the amount of heat that is conducted in a material. If an area of low conductivity is studied, Fourier's law tells that the geothermal gradient (discussed in Section 2.2.3) must be increased if the heat flux is constant in that area. In other words, geothermal anomalies can be related to the variations of the thermal conductivity of rocks.

The thermal conductivity of rocks varies with several factors. Pressure, pore fluids, the dominant mineral in the rock and degree of saturation are some of these factors [Clauser and Huenges, 1995]. Air and water have relatively low conductivity, $0.024 W m^{-1} K^{-1}$ and $0.6 W m^{-1} K^{-1}$ respectively [Banks, 2012]. If a rock has large pores filled with air or water, the thermal conductivity of the rock will be low. The rock forming mineral, quartz, has high thermal conductivity, $7.8 W m^{-1} K^{-1}$ [Banks, 2012]. Rocks with a high amount of quartz will therefore have high thermal conductivity. Examples of rocks with high thermal conductivity due to the high amount of quartz are granite ($3.0 - 4.0 W m^{-1} K^{-1}$), gneiss ($2.5 - 4.5 W m^{-1} K^{-1}$) and quartzite ($5.5 - 7.5 W m^{-1} K^{-1}$) [Banks, 2012].

Figure 2.12 shows how the geothermal gradient change in a cross section of granite, mudstone and sand. Here one can see that granite has the highest thermal conductivity and therefore the geothermal gradient is less here than in the layer of sand or mudstone.

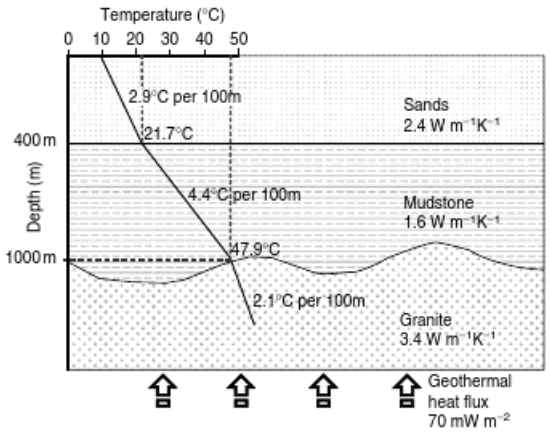

Figure 2.12: *Geothermal gradient in a cross section [Banks, 2012]*

Groundwater Groundwater can also contribute to increasing the geothermal potential in an area. Groundwater can transport heat from one location to another, as shown in Figure 2.13.

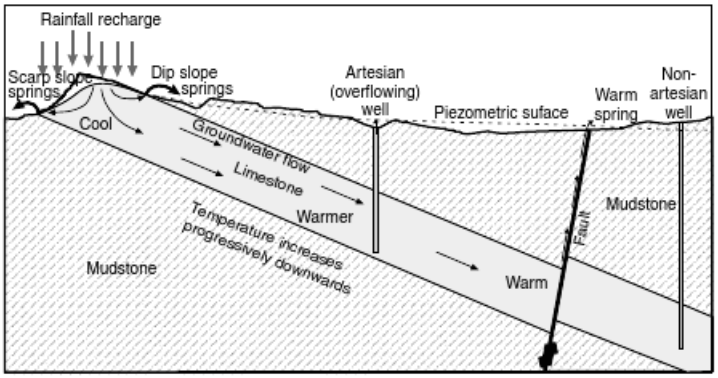

Figure 2.13: *Groundwater flow in limestone [Banks, 2012]*

A layer of permeable and porous material where groundwater can flow are called an aquifer [Lutgens et al., 2009]. In Figure 2.13 the layer with water saturated limestone is an aquifer. The surrounding mudstone has lower permeability and is less porous, and therefore the groundwater is trapped within the layer of limestone.

The geothermal, gradient discussed in Section 2.2.3, contributes to increase the temperature of the groundwater. The groundwater flow transports heat by convection (discussed in Section 2.1.4). A fault in the ground allows the hot groundwater to naturally escape to the surface. This will result in a warm spring. An artesian well will also transport the water from the deep to the surface. If the pressure in the aquifer is high enough, the water will naturally escape to the surface because of the pressure difference, and the well will overflow. The well to the left in Figure 2.13 is an example of an overflowing artesian well.

Internal heat production Some rocks have internal heat production that can contribute to a local increased geothermal gradient. The internal heat production in a rock can be caused by radioactivity (discussed in Section 2.1.3) or chemical reactions within the rock. The minerals in a coal deposit, such as pyrite (FeS_2), marcasite (FeS_2), sphalerite (ZnS) and galena (PbS), all oxidise when they are exposed to air and water [Banks, 2012]. The oxidisation produces heat which causes the local geothermal gradient to increase. Granite is an example of a rock with high internal heat production and is therefore a good target for hot dry rock geothermal systems. High enthalpy geothermal system are discussed in Section 2.3.4.

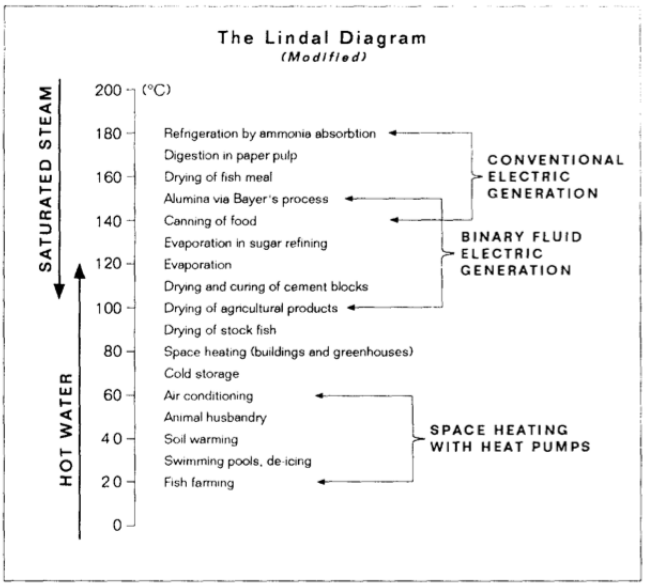

Figure 2.14: *Modified Lindal diagram from [Fridleifsson and Freeston, 1994]*

2.3 Technology

2.3.1 Geothermal systems

It is normal to classify geothermal systems based on enthalpy. Enthalpy is defined in Section 2.1.1 and is closely related to temperature and pressure. There are two main types of geothermal systems, low enthalpy systems and high enthalpy systems. Low enthalpy systems are related to shallow geothermal systems and high enthalpy systems are related to deep geothermal systems.

The utilization of geothermal fluids depends on the temperature of the geothermal fluid extracted from the system. A Lindal diagram [Lindal, 1973] shows the required temperatures of the geothermal fluid for use in different applications. A modified version of the Lindal diagram is shown in Figure 2.14.

As shown in Figure 2.14, geothermal fluids with temperature below $100°C$ is used for space heating. These types of geothermal systems are shallow geothermal systems. Geothermal systems with geothermal fluids above $100°C$ is used for production of electricity, and are normally deep geothermal systems. The different factors that control the temperature of the geothermal fluids are discussed in Section 2.2.4. Island is a well known location that

produces electricity from geothermal fluids. Island is located on a divergent plate margin, and therefore hot geothermal fluids are accessible at shallower depths.

Shallow geothermal systems and deep geothermal systems are discussed in more detail in Section 2.3.3 and Section 2.3.4.

2.3.2 Heat pump

A heat pump is an engine that uses mechanical energy to transmit heat from a cold reservoir to a hot reservoir. The second law of thermodynamics (discussed in Section 2.1.1) states that heat tends to flow from hot to a cold reservoirs. A heat pump must therefore use mechanical energy to make the heat go from the cold reservoir to the hot reservoir.

The combined heating effect from the reservoir in the geothermal system, and the heat pump, can be calculated by using the following equation [Banks, 2012]

$$H \approx G + E \tag{2.24}$$

where H is the total heating effect [W], G is the heat extracted from the ground [W] and E is electrical power input to the heat pump [W].

The efficiency of a heat pump is normally termed as the coefficient of performance (COP). The COP can be calculated from the following equation [Schroeder, 2000]

$$COP = \frac{H}{E} \tag{2.25}$$

where H is the amount of heat delivered and E is the electrical energy used by the heat pump. Note that the COP is normally denoted with an H when the heat pump is used for heating, and C when it is used for cooling.

If a ground source heat pump is used for space heating, one wants the COP_H to have a value above 3 [Banks, 2012]. The COP can vary over time. The seasonal performance factor (SPF) is used to calculate the efficiency of a heat pump over time. The SPF is a long term average of the COP.

Ground source heat pump

A ground source heat pump uses the heat from a geological environment [Banks, 2012]. This type of heat pump is the most common heat pump used to extract geothermal energy. There are two main types of ground source heat pumps; open- and closed loop ground source heat pumps.

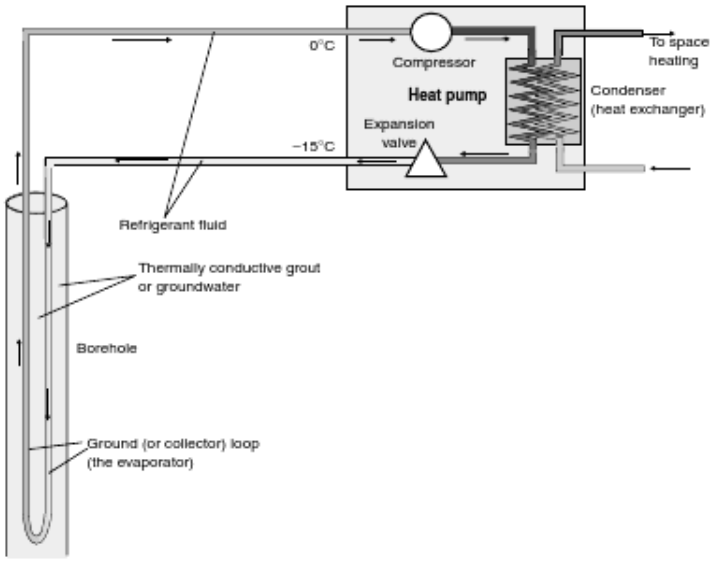

Figure 2.15: *Direct circulation closed loop heat pump scheme [Banks, 2012]*

Open loop ground source heat pumps uses water from a natural source, such as water from a lake or a river, or groundwater. If the groundwater flow rate, Z $[m^3 s^{-1}]$, and the temperature drop across the heat pump, $\Delta\theta$ [K], is known, we can calculate the heat extracted from the ground by using the following equation [Banks, 2012].

$$G = Z \times \Delta\theta \times S_{VC_{water}} \tag{2.26}$$

Where, $S_{VC_{water}} = 4180 Jm^{-3}K^{-1}$ is the volumetric heat capacity of water. Note that the volumetric heat capacity of water is dependent on the temperature of the water.

There are two types of closed loop ground source heat pumps. Direct circulation systems uses a refrigerant fluid in the heat pump as the circulating fluid in the pipes. An illustration of an direct circulation closed loop heat pump is shown in Figure 2.15.

An indirect circulation system uses two different fluids, a carrier fluid that circulates in the pipes and a refrigerant in the heat pump. Figure 2.16 shows an illustration of an indirect circulation closed loop scheme.

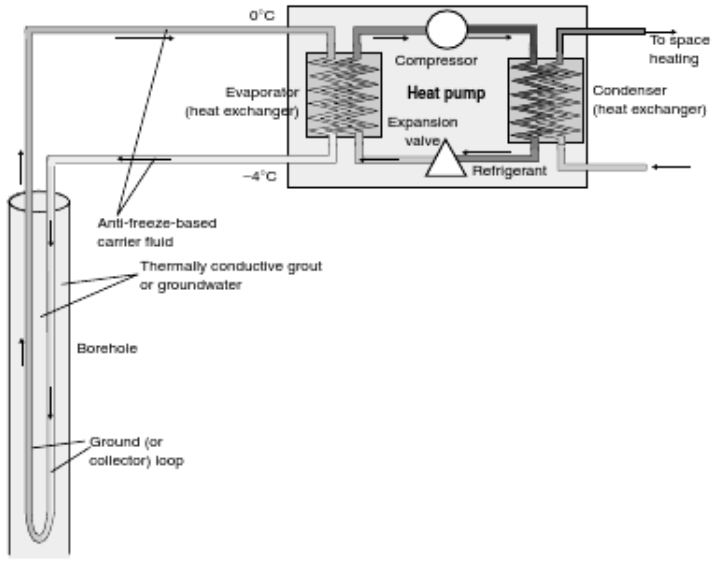

Figure 2.16: *Indirect circulation closed loop heat pump scheme [Banks, 2012]*

2.3.3 Shallow geothermal systems

Shallow geothermal systems uses the upper 250 m of the earth as heat source [Ramstad, 2011]. For shallow geothermal systems, the temperature that is extracted from the ground is normally too low for electricity production. Shallow geothermal systems are therefore used for heating purposes.

In all shallow geothermal systems, a heat exchange fluid called the carrier fluid, circulates in the pipes [Banks, 2012]. The carrier fluid is normally a mixture of water and an antifreeze solution [Huttrer, 1997]. The carrier fluid is heated by the ground by conduction (described in 2.1.4), and this creates a temperature difference between the carrier fluid entering and leaving the system. By forced convection (described in 2.1.4), the hot water can be transported to a ground source heat pump which can lift the temperature difference to achieve the temperature that is required for the heating purpose. The heat pump also ensures that the carrier fluid enters the system with the same temperature on every loop. The carrier fluid can also be used directly for heating purposes without a heat pump.

The earth's most important heat source is the sun. The heat from the sun can only penetrate the subsurface to a certain point. Below 10 meters, the temperature of the ground is stable throughout the year [Banks, 2012]. The air temperature effects the temperature of the upper part of the subsurface. The subsurface temperature will therefore depend on the elevation and the

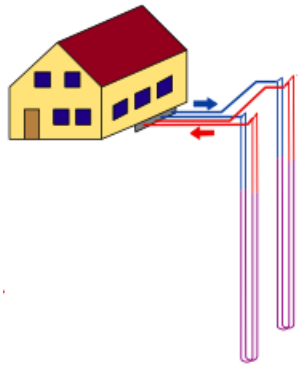

Figure 2.17: *A vertical geothermal system [Hellström, 2011]*

climate where the geothermal system is located, since the air temperature is strongly connected to these two factors.

The subsurface is able to store heat. In summer, when incoming solar radiation is high, the subsurface temperature increases and this heat is stored in the ground. The temperature of the subsurface will therefore be higher than the air temperature at winter season and lower at summer season [Omer, 2008].

As mentioned, the incoming solar radiation only effects the upper 10 meters of the subsurface. Other sources that effects the ground temperature, as internal heat production in rocks, difference in the thermal conductivity of rocks and groundwater as well as tectonics, are all discussed in Section 2.1.3.

In all shallow geothermal systems, good circulation in the pipes are important to have high heat transfer from the ground to the carrier fluid. A water pump is installed to make the fluid circulate through the pipes [Banks, 2012].

Vertical geothermal systems

A typical vertical system consists of two straight pipes connected in the bottom forming a U-shaped pipe. The vertical geothermal system in Figure 2.17 has two boreholes with two U-shaped pipes in each borehole. Both the number of pipes and the number of boreholes in a vertical geothermal system depends on the size and purpose of the system. For a household, one borehole with one U-shaped pipe can be enough, but for a bigger building, for example a large office or an industry building, several boreholes and pipes are necessary to extract the sufficient amount of energy.

The depth of the well also influences on the amount of energy that can be

extracted from the system. A deeper well can extract higher temperatures than a shallow well. A typical geothermal system with vertical wells has a depth between 20 and 300 meters [Pahud and Matthey, 2001]. The depth of a well in a vertical geothermal system depends on the geological environment in the area and the purpose of the system. The economical aspect is also an important factor for the depth of the well, as increasing depth will increase the cost of drilling.

To extract as much energy as possible from the ground, the design of the well is crucial. The pipe material must be a material with high thermal conductivity, such that the heat from the ground can easy warm the carrier fluid. The pipes are usually made of high density polyethene, which have high thermal conductivity [Banks, 2012]. It is also important that the pipes are in good contact with the ground. To ensure this, it is normal to fill the borehole with a material that also has a high thermal conductivity [Banks, 2012].

Normally, U-shaped pipes have an outer diameter of 32-40mm, and are installed with a spacing of 90-110mm between the two pipes [Banks, 2012]. To maintain this spacing in the borehole, clips are used to avoid the two pipes to get in thermal contact with each other [Hellström, 2011]. If there are several boreholes, the spacing between the boreholes also influences on the heat extraction from the ground. In cold northern climates, the spacing between the boreholes should be more than 4.6 meters apart to achieve this [Omer, 2008].

A vertical geothermal system can use a closed ground source heat pump, described in Section 2.3.2. Both direct and indirect circulation loops can be used in a vertical system.

Horizontal geothermal systems

Vertical geothermal systems are favoured in urban areas, as they do not claim a big surface area. Drilling a vertical well is more expensive than drilling a horizontal well. If surface area is not a limitation, a horizontal geothermal system is favoured [Omer, 2008]. In a horizontal geothermal system, the pipes are buried in a trench 1.2 - 2 m under the surface [Sanner, 2011]. In cold climates the ground may freeze at this depth during the winter. Frost is not desired, since it can destroy the system. Both the depth and the length of the pipes depends on the purpose of the system. A large system need deeper and longer pipes, since the desirable temperature difference for a large system is higher than a small system.

Figure 2.18 shows two different arrangements of a horizontal systems. One

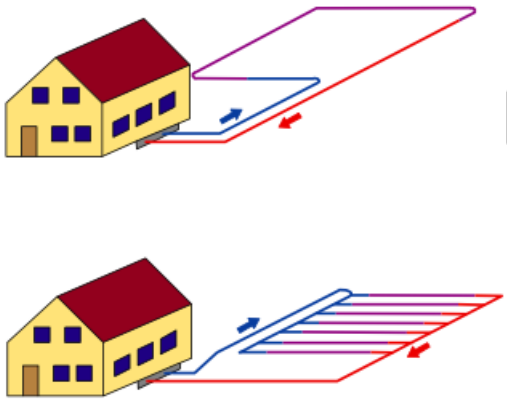

Figure 2.18: *The upper horizontal geothermal system has one pipe in a trench, and the bottom system has pipes connected in parallel [Sanner, 2011]*

way to minimize the area of the horizontal system is to have several pipes in a dense patters, either in series or in parallel [Omer, 2008]. In Figure 2.18 the bottom horizontal system has pipes connected in parallel. The upper system in the figure is a horizontal system with pipes in a trench. There are several other ways to design a horizontal geothermal system [Banks, 2012].

Just as in a vertical geothermal system, the pipes in a horizontal geothermal system are usually made of polyethene. Both medium and high density polyethene can be used in a horizontal system [Banks, 2012]. To ensure good heat transfer between the pipes and the ground, it is important to fill all the air filled pores around the pipe with a material with good thermal conductivity [Banks, 2012]. The main heat source for the ground surrounding a horizontal geothermal system is the sun.

Horizontal geothermal systems are closed loop systems, and both ground source heat pumps with direct and indirect circulation loops can be used in a horizontal system.

Pond and lake systems

Instead of extracting heat from the ground, it can be extracted from a pond or a lake. These types of systems can either be open or closed. A closed pond system is very similar to a horizontal geothermal system, except that the pipes are located in a pond instead of the ground. The pipes in a closed loop pond system are usually made of high density polyethene, and the carrier fluid in the pipes have typically an initial temperature $3 - 5°C$ lower than the temperature of the pond [Banks, 2012]. The carrier fluid in the pipes

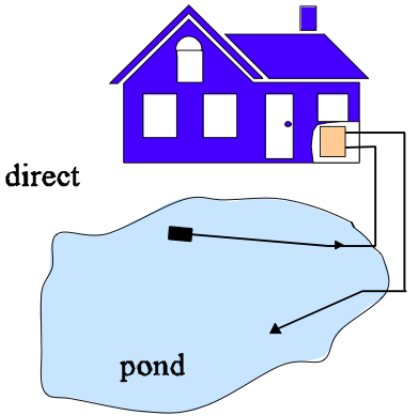

Figure 2.19: *Open loop pond system [Lund* et al.*, 2004]*

will absorb heat from the water in the pond by conduction (Section 2.1.4). The heated carrier fluid circulates through the pipes in the pond and finally to a heat pump through an insulated tube. The heat pump extracts energy from the heated carrier fluid.

Figure 2.19 shows an open loop pond system. An open loop pond system is very similar to a groundwater system described in the next section. In an open loop pond system there is one extraction well and one injection well. The extraction well pumps the water from the pond to the heat pump. To prevent large temperature difference in the pond and that the pond dries out, the water is reinjected after the heat has been extracted.

It is important for all pond based system that both the temperature and the water level in the pond is not influenced too much. If this happens, the ecological environment in the pond can be destroyed [Banks, 2012].

Geothermal systems based on groundwater

Geothermal systems based on groundwater are open loop systems. In a groundwater system, two vertical pipes are drilled in the ground, similar to a vertical system, only here the loop is open. One of the wells are a production well and the other a injection well.

Groundwater system can only be installed in areas with groundwater available in the subsurface. Rocks or sediments in the subsurface that are able to contain groundwater are called an aquifer [Banks, 2012]. An aquifer is a rock with high porosity and permeability, for example sand. A rock that prevents

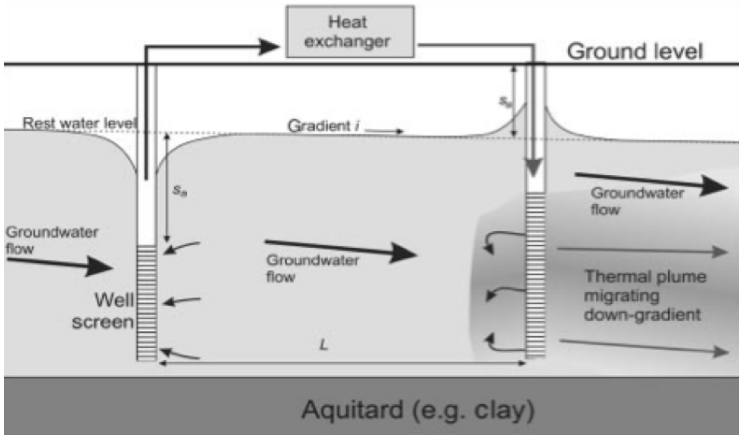

Figure 2.20: *A groundwater system with one production well and one injection well [Banks, 2012]*

groundwater to flow through it, because of low porosity and permeability, are called an aquitard [Lutgens et al., 2009].

The groundwater level is affected by a groundwater system. The groundwater level changes when water is extracted and injected. Around the production well, where the groundwater is extracted, there will be a cone of depression [Lutgens et al., 2009]. Around the injection well the groundwater level will be higher than the normal level, an inverse cone of depression. It is important to map the natural groundwater flow before a groundwater based system is installed. The water from the reinjection well must flow away from the production well, so that the reinjected water not is used in the production well [Banks, 2012]. Because of the reinjection of water, there might occur a reversed groundwater flow in the opposite direction of the natural groundwater flow. In Figure 2.20 one can see that the water from the reinjection well flows away from the production well.

2.3.4 Deep geothermal systems

High enthalpy systems utilize geothermal fluids with high temperature and pressure. The geothermal fluid in a high enthalpy system is normally above $100°C$ [Boyle, 2004]. To achieve this temperature, high enthalpy systems are normally deep systems. The depth that is required in a high enthalpy geothermal system vary, depending on the geology in the area and the purpose of the system.

Turbines are used to generate electricity from the steam extracted from the geothermal well. To generate electricity directly from the steam, the geother-

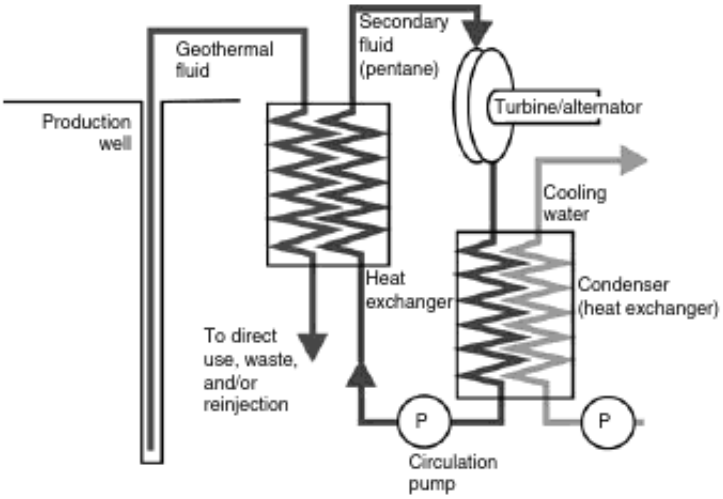

Figure 2.21: *Binary system that produces electricity with geothermal fluid below* $100°C$ *[Banks, 2012]*

mal fluid must have a temperature above $150°C$ [Banks, 2012, Fridleifsson and Freeston, 1994]. It is still possible to produce electricity from geothermal fluids with lower temperature. The Lindal diagram, Figure 2.14, shows that electricity production is possible with geothermal fluids at temperatures down to under $100°C$. This is possible when a secondary fluid is circulated through the turbine instead of the geothermal fluid. The geothermal fluid heats the secondary fluid, which has a low boiling point. Figure 2.21 shows a binary system that produces electricity.

Rocks with low permeability and porosity are normally not suitable for geothermal systems. Granite is an example of a rock with low permeability and porosity. Granite has high internal heat production, as mentioned in Section 2.2.4. Geothermal systems that contains rocks like granite are called hot dry rock systems. To increase the permeability and porosity of the rock, artificial cracks are made by using explosives in a borehole. When the permeability and porosity have reached the required demand, water is pumped down in the rock. The water circulates through the cracks in the hot rock, and the heated water is finally pumped to the surface through a second borehole.

Chapter 3

Ny-Ålesund

3.1 Energy consumption and demand in Ny-Ålesund

3.1.1 Energy production

Today, a diesel generator fulfills the energy demand to the small community in Ny-Ålesund. To produce electricity in a diesel generator, oil or gas are injected in to a motor or a turbine which powers an electrical generator. This process generates heat. Normally, in this power generation process, 30-40 % of the energy content in the fuel are converted into electricity, 40-50 % are converted into heat and the rest is lost as heat to the surroundings. There are several options for generate extra electricity or heat if needed, in addition to the process described above. Electricity can also be converted in to heat in an electric boiler, or heat can be generated by burning fuel in an oil boiler. Another opportunity are to cool the excess heat. The power station in Ny-Ålesund uses all these three options. The oil boiler in Ny-Ålesund were installed in 1982 and have a capacity of 810 kW, but the connected burner only has a capacity of 470 kW. The electric boiler in Ny-Ålesund has a capacity of 225 kW [Jørgensen and Bugge, 2009].

The power station in Ny-Ålesund, which were installed in 1997, consists of three diesel generators which have 500 kW electricity effect each [Jørgensen and Bugge, 2009]. The diesel generators produce electricity used for equipment and heating. In the last years the total diesel consumption have been $1000 - 1200m^3$, and this corresponds to an energy production of 10 - 12 GWh per year [Jørgensen and Bugge, 2009]. The total consumption of diesel in 2005 was $1131m^3$ [Shears et al., 1998]. Diesel are supplied twice a year, and the diesel are stored in two cylindrical containers with a total capacity of $1100m^3$.

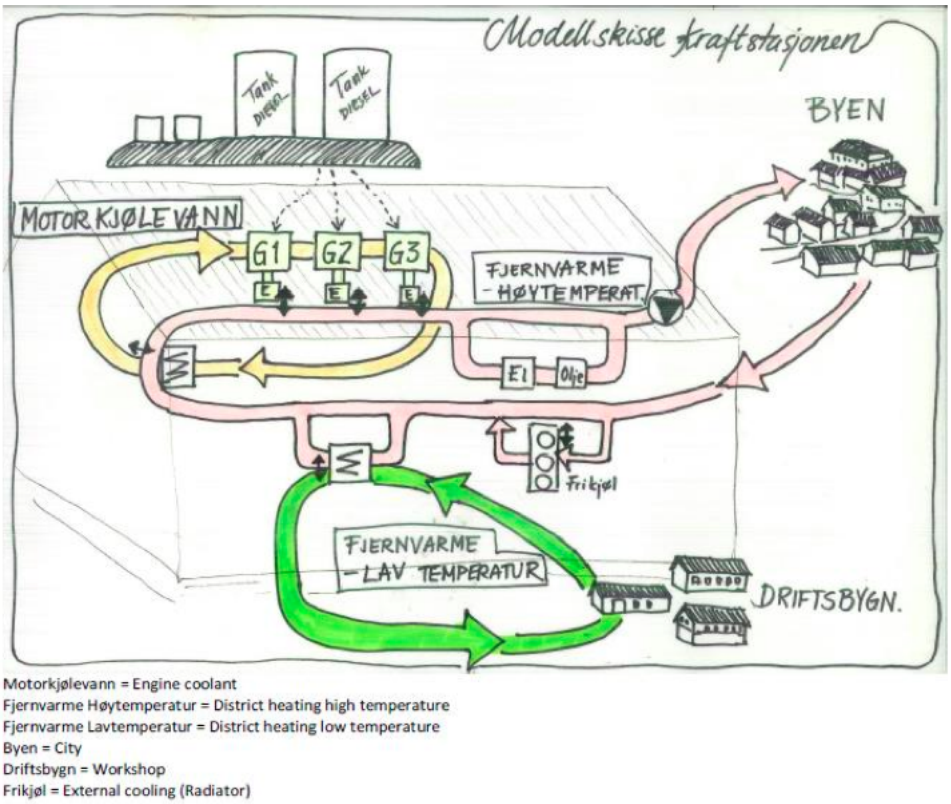

Figure 3.1: *Schematic drawing of the district heating system in Ny-Ålesund [Midttømme* et al.*, 2013]*

Normally, only one of the three generators are in use [Jørgensen and Bugge, 2009]. In periods when the energy demand is large, two of the generators are used simultaneously. The third generator are in standby most of the time. It is not desirable to start up the second generator for short periods of time, both from an energy and operational point of view. There are also an emergency generator unit in Ny-Ålesund with capacity of approximately 188 KW [Jørgensen and Bugge, 2009].

The excess heat from the power station is distributed in a district heating system, shown in Figure 3.1. The system consists of one high temperature and one low temperature circuit. The high temperature water is circulated through the city, while the low temperature water is used in the service buildings. To maintain a sufficient temperature difference in the system, the return water in the high temperature heats the low temperature circuit. This increases the efficiency of the system.

	GWh	**kW**
Heating	4.8	1200
Cooling	0.2	
Electrical	4.1	700

Table 3.1: *Effect and energy demand in Ny-Ålesund in 2005 [Jørgensen and Bugge, 2009]*

3.1.2 Energy consumption

There are about 70 buildings in Ny-Ålesund and approximately half of them are heated to room temperature during the whole year [Jørgensen and Bugge, 2009]. The diesel consumption and the energy consumption in Ny-Ålesund was stable in the years 2000-2005. The total energy demand in Ny-Ålesund in 2005 are summarized in Table 3.1.

The heating demand is strongly dependent on the outside air temperature. The outside air temperature are shown in Figure 3.2. Because of the cold temperatures in winter, the heating demand is naturally increasing in the winter months. The demand for electricity also increases in winter, because some of the heating equipment rely on electricity.

Another aspect that effects the energy consumption in Ny-Ålesund is that the population vary during the year. In summer, there is about 150 inhabitants in Ny-Ålesund. In winter, this number decreases to only 30 [Shears et al., 1998]. The total number of researchers in visiting Ny-Ålesund has increased, and the increasing activity in Ny-Ålesund implies a higher energy demand. If the activity in Ny-Ålesund is continuing to increase, a new energy source which can provide heat to the community is desirable.

3.2 Climate

The archipelago of Svalbard ranges from $74° - 81°$ north. There are big difference in the climate in the north and the south of the archipelago, as well as the east and the west coast. Both warm and cold sea current strikes Svalbard, and the sea currents have a great effect on the climate on the archipelago.

Because of the warm north Atlantic current, Svalbard's climate is moderate compared to other locations on the same latitude. The north Atlantic current strikes the west coast of Svalbard, and contributes to a warm and milder climate. The climate on the east coast of Svalbard is influenced by

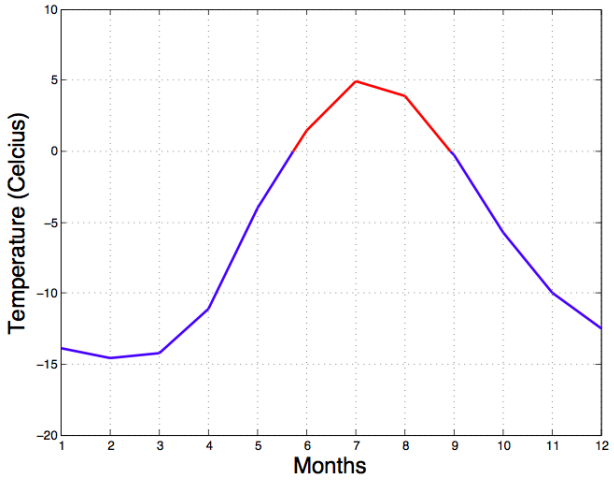

Figure 3.2: *Average annual temperature in Ny-Ålesund. Data from [eKlima, 2013]*

the cold Siberian currents, and therefore the climate here is colder than at the west cost.

3.2.1 Temperature and precipitation

Figure 3.2 shows the mean annual air temperature in Ny-Ålesund. The average air temperature in Ny-Ålesund in the period 1961 to 1990 was $-6.3°C$ and from 1981 to 2010 the average air temperature was $-5.2°C$ [Førland et al., 2011]. Since Ny-Ålesund is located far north, the incoming solar radiation is low, as described in Section 2.1.3.

The annual precipitation in Ny-Ålesund is low. From 1961 to 1990 the total precipitation was 385 mm and the total precipitation from 1981 to 2010 was 427 mm [Førland et al., 2011].

3.2.2 Permafrost

If the ground remains below $0°C$ over at least two years, it is defined as permafrost [Harris, 1988]. About one fourth of the land surface on the Northern hemisphere is permafrost regions. However, permafrost may not be present everywhere in the permafrost regions. It is estimated that approximately 15 % of the land on the nothern hemisphere is underlain by permafrost [Zhang et al., 2000]. 60 % of Svalbard is covered by glaciers. The remain-

Figure 3.3: *Permafrost areas on Svalbard. The grey areas indicates ice free permafrost regions. [Humlum* et al.*, 2003]*

ing 40 % (approximately $25000 km^2$) is permafrost regions. Outside Russia, Svalbard is the largest permafrost area in Europe [Humlum et al., 2003]. Figure 3.3 shows the permafrost areas on Svalbard.

The main factors that controls the permafrost distribution are air temperature, soil moisture, topography, lithology, snow cover, geothermal heat flow and distance to the ocean [Humlum et al., 2003]. The depth of the permafrost on Svalbard varies from 450 m in the highlands to less than 100 m close to the shore [Liestøl, 1980]. In summer, when the air temperature is above freezing, the upper permafrost layer melts. The fluctuations in air temperature during the year does not effect the temperature in the ground below 15-20 m [Sollid et al., 2000]. Below this level, the geothermal gradient is $2 - 3°C$ per 100 m [Liestøl, 1980].

Measurements and analysis of the changes in the permafrost, can revile systematic changes in the ground temperature and heat balance, as well as detecting climate changes. The thickness of the permafrost will not be influenced by climatic changes on a short time period, but the groundwater

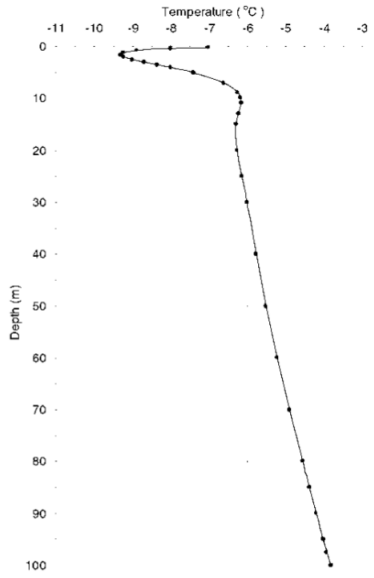

Figure 3.4: *Temperature profile on Janssonhaugen [Sollid* et al.*, 2000]*

recharge and discharge will be strongly effected [Haldorsen and Lautitzen, 1993]. Long time climate changes can be revealed in changes in the permafrost. The permafrost works as an archive of the climate of the past [Sollid et al., 2000].

In May 1998 a borehole in Janssonhaugen in Avdentdalen ($78°10'46''N$, $16°28'01''E$) was drilled to determine the permafrost thickness and the temperature gradient [Sollid et al., 2000]. The average annual temperature on the site was $-8.0°C$ and the average annual precipitation was 300 - 500 mm. The borehole site was located at 270 meters above sea level. The temperature in the borehole on May 9th 1999, a year after the drilling, is shown in Figure 3.4.

The effects from the seasonal variation of the air temperature can be seen in the upper 20 m in Figure 3.4. The zero annual amplitude depth of the site on Janssonhaugen is 18 m below the surface and the permafrost thickness is estimated to 220 m [Isaksen et al., 2001]. Palaeoclimatic analysis on the temperature profile in Janssonhaugen shows that there have been a notable warming of the subsurface during the twentieth century [Isaksen et al., 2001].

Permafrost in Ny-Ålesund

The permafrost in Ny-Ålesund is thinner than on Janssonhaugen. In general, the permafrost thickness on the inland is thicker than on the coast. In Ny-Ålesund, the lower limit of the permafrost has varied in time. During the last mining period in Ny-Ålesund, the thickness of the permafrost was measured near the foot of Zeppelinfjellet. At that location, the lower permafrost limit was at a level between 0 and 50 m below sea level, or 50 - 100 m below the ground surface [Haldorsen and Lautitzen, 1993]. The groundwater conditions in Ny-Ålesund effects the permafrost thickness. This is discussed in Section 3.3.3.

3.3 Geology

3.3.1 Geology of Svalbard

Figure 3.5 shows the geology on Svalbard. The earth's history can be revealed by understanding the geology, and Svalbard is one of few places on earth where geology from most sections that reviles the earth's history is easy accessible.

The oldest rocks on Svalbard are contained within the basement and these rocks are dated to 3.3 billion years [Elvevold et al., 2007]. The rocks in the basement were formed in Precambrian to Silurian time. The basement mainly consists of igneous and metamorphic rocks which have been folded and have experienced metamorphism throughout time. The basement is present on several locations on Svalbard, for example on the west coat.

The sedimentary rocks are younger than the basement. The sedimentary rocks were deposited during Carboniferous to Permian time. These types of sedimentary rocks can be found on several locations on Svalbard. Deposits from the Quaternary period also dominate the geology on Svalbard. Deposits from the last ice age, like moraines and fluidal deposits are common all over Svalbard.

Svalbard is located on the edge of the Eurasian plate. The different tectonic plates and the plate margins are all shown in Figure 2.7. There is no volcanic activity on Svalbard today, but the last period of active volcanism on Svalbard are dated between 1 million and 100 000 years ago. This volcanic activity was caused by a hot spot located north-west of Spitsbergen. Quaternary volcanic rocks can be found on several locations, one of them near Bockfjorden north-west on Spitsbergen. Here, one can also find several thermal

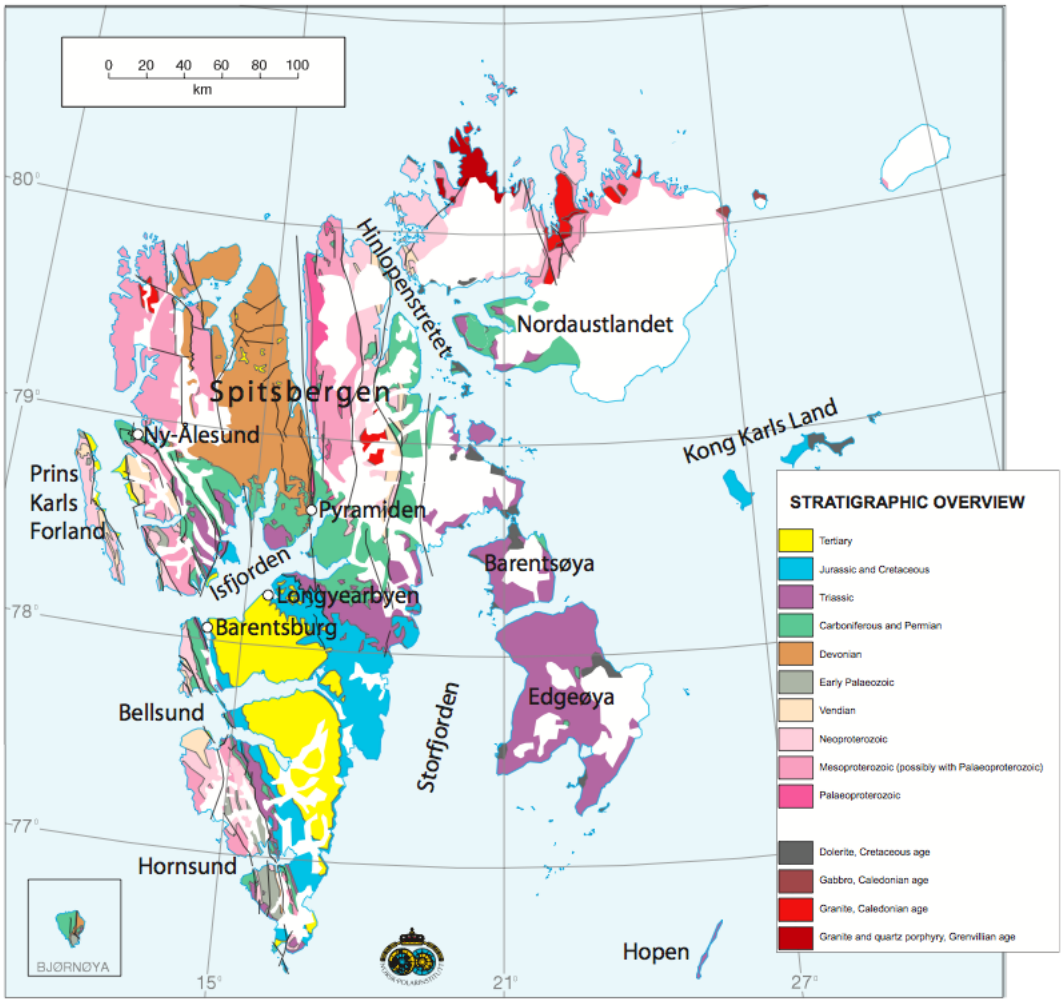

Figure 3.5: *Geological map of Svalbard [Elvevold* et al.*, 2007]*

springs with water that holds a temperature of $24°C$ [Elvevold et al., 2007]. Thermal springs are not common on Svalbard. Permafrost is dominating, and the thickness of the permafrost ranges from less than 100 m close to the sea to more than 500 m in the highlands [Humlum et al., 2003]. The distribution of permafrost on Svalbard is described in Section 3.2.2.

Figure 3.6: *Geological map of the area around Ny-Ålesund. Segment from [Hjelle* et al., *1999]*

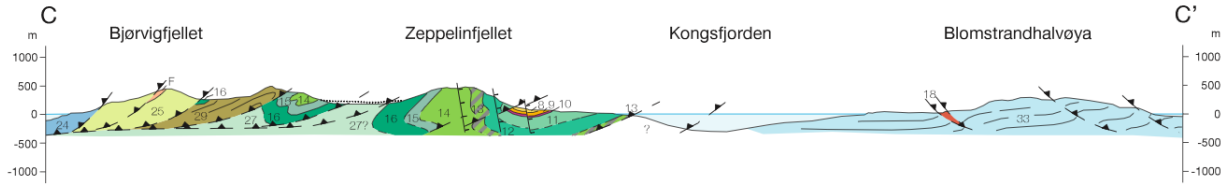

Figure 3.7: *Cross section C-C' from Figure 3.6 [Hjelle* et al.*, 1999]*

3.3.2 Geology near Ny-Ålesund

Ny-Ålesund is located on the northern side of Bøggerhalvøya. The area is dominated by an alpine upland area with mountain peaks up to 600 m above sea level. Glaciers in the valleys flow down from the mountains to the coastal plains near the sea. Bøggerbreen and Lovenbreen is the two glaciers closest to Ny-Ålesund. Bøggerbreen to the southwest is $8km^2$, and Vestre Lovenbreen to the southeast is $4km^2$.

Figure 3.6 shows the different deposits near Ny-Ålesund. The area are dominated by several normal faults. The faulted rocks marked as orange and pink (8, 9 and 10) are mainly sandstone, shale and conglomerate from Paleocene and early Triassic. The Bøggerbreen Formation, marked as 8, and the Kongsfjorden Formation, marked as 9, contain coal which were mined in Ny-Ålesund from 1917 to 1962.

The rocks in the Kapp Starostin Formation is a part of the Tempelfjorden Group and are marked as 11 in Figure 3.6. These rocks are dated to late Permian and consists of siliceous shale, chert, limestone and sandstone. The thickness of this sequence is approximately 200 - 300 m [Hjelle et al., 1999] and have a porosity of 12 - 19 % [Booij et al., 1998].

The rocks that are marked with 12 in Figure 3.6 are the Gipshuken Formation which is a part of the Gipsdalen Group. This formation consists mostly of dolomite breccia, dolomite, limestone and marl [Hjelle et al., 1999]. The Gipshuken Formation has a thickness of 130 - 140 m [Hjelle et al., 1999] and a porosity of 1 - 15 % [Booij et al., 1998].

The rock marked as 13 in Figure 3.6, the Wodiekammen Formation, are also a part of the Gipsdalen Group. The Wordiekammen Formation contains dolomite and limestone and the formation has a thickness of maximum 300 m [Hjelle et al., 1999]. The age of the Gipsdalen Group is middle Carboniferous to early Permian.

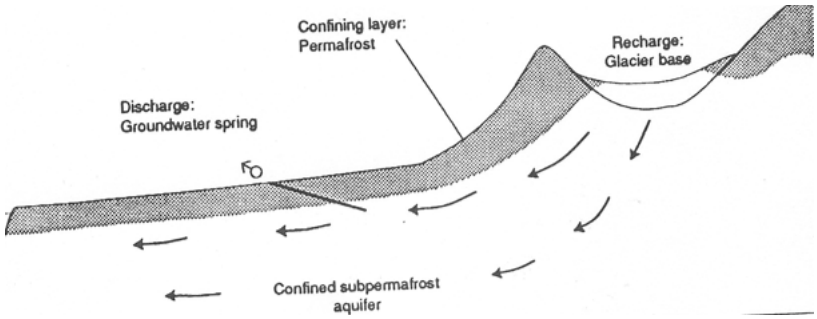

Figure 3.8: *Groundwater flow in Ny-Ålesund. Shaded area show where the permafrost is present. The direction of the profile is NNE - SSW [Haldorsen* et al.*, 1996]*

Around Ny-Ålesund there are several moraines and fluvial deposits from the Quaternary period. The moraines are marked as white with dots (1), while the fluvial deposits and marine shore deposits are marked with light pink (2 and 3).

On Blomstrandhalvøya in Kongsfjorden the basement are present. The rocks here are mainly marble from Proterozoic. Figure 3.7 shows the rocks in the subsurface down to approximate 500 meters. The reversed fault in Kongsfjorden may indicate that the basement present on Blomstrandhalvøya continues under Bøggerhalvøya. This is not certain, because of complicated faulting in the area. This is indicated in Figure 3.7 with a question mark.

3.3.3 Groundwater conditions in Ny-Ålesund

In Ny-Ålesund, the groundwater flows in subpermafrost aquifers. Figure 3.8 shows the groundwater system in Ny-Ålesund. The main recharge area is the glacier Vestre Lovenbreen and the main discharge is the Easter mine. The permafrost is the confining layer in the groundwater system. The groundwater system is dependent on the geological conditions in the area where high porosity and permeability of the rocks are required for groundwater to flow. The groundwater system is also dependent on the climate [Haldorsen et al., 1996]. Both recharge and discharge of groundwater require an opening in the permafrost. The thickness of the permafrost layer, which is the confining layer in the groundwater system, defines the upper limit of the groundwater flow. The recharge area and the recharge rate defines the amount of groundwater present. The glaciers size and properties decides the recharge rate at the base of the glacier.

Groundwater recharge

Glaciers have a large influence on the groundwater level. All glaciers on Spitsbergen are of a subpolar type [Liestøl, 1980]. A glacier of subpolar type have temperatures above freezing in the accumulation area. This causes the melting water to sink to the base of the glacier and further downwards under the permafrost layer, locally creating an opening in the permafrost. In the main melting periods, during summer, most of the melting water will emerge in the front of the glacier. The main recharge for the groundwater in Ny-Ålesund is from the two glaciers nearby, Bøggerbreen and Lovenbreen [Haldorsen et al., 1996]

Lakes will have a great influence on the groundwater level, which in turn influences the permafrost level. If a lake is less than 400 m across, the permafrost will form a continuous layer under the whole lake [Liestøl, 1980]. If this is the case, there will not be a groundwater flow under the lake. The two lakes near Ny-Ålesund, Tvillingvatn and Storvatnet, are both small and less than 400 m across. It is therefore assumed that the permafrost is continuous beneath both lakes and that the lakes does not provide recharge to the groundwater system [Booij et al., 1998].

Groundwater discharge

During the two mining periods in Ny-Ålesund, groundwater was observed in some of the mines. The inflow of groundwater was a big problem and some places the groundwater flooded the mines. The two normal faults closest to the settlement in Ny-Ålesund, the Agnes fault to the east and the Josefine fault to the west, both penetrates the rocks that were mined. The groundwater inflow from these faults were observed to be 15 - 40 liters per second, and the water inflow was always from below [Haldorsen and Lautitzen, 1993]. Groundwater has also been observed within the permafrost zone, above the lower limit of the permafrost, along the fault zone. The temperature of the groundwater below the permafrost is about $3°C$ [Haldorsen and Lautitzen, 1993].

The main discharge point for the groundwater is from a spring in one of the coal mines, The Easter spring. The Easter spring is shown in Figure 3.6 and Figure 3.9. Since the last mining period it has been observed a continuous discharge of groundwater here [Haldorsen et al., 1996]. During the summer and fall in 1993 and 1994 a flow rate of 11.5 liters per second, or 365 000 $m^3/year$, were observed in the Easter spring [Haldorsen et al., 1996]. Groundwater discharge may be higher than it naturally would have been because of the mining. The Easter spring is a result of mining, and the continuous groundwater flow in the spring during the mining period have

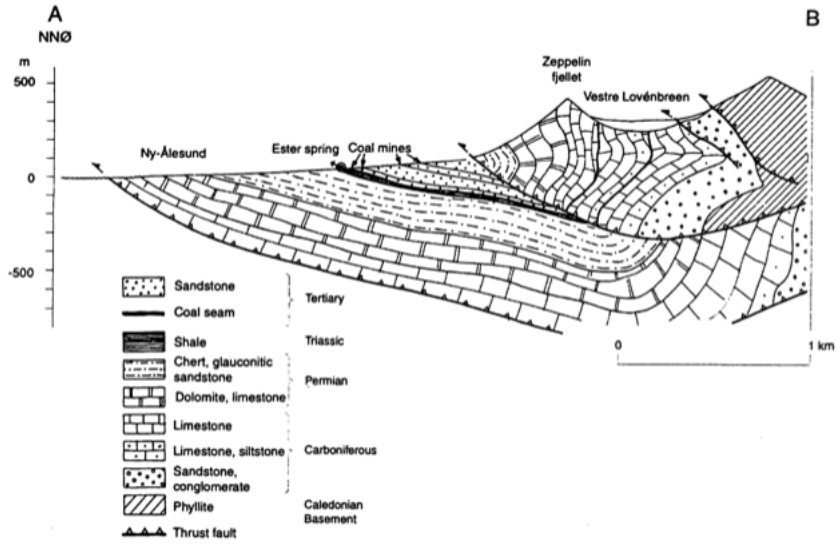

Figure 3.9: *Bedrock profile in Ny-Ålesund. The direction of profile is NNE - SSW, in the assumed direction of the groundwater flow [Booij* et al.*, 1998]*

caused the permafrost to melt [Haldorsen et al., 1996].

Aquifers

Subpermafrost groundwater are found in Ny-Ålesund. The groundwater in Ny-Ålesund is found in the sandstone marked as 11 in Figure 3.6 [Haldorsen and Lautitzen, 1993]. The physical characteristics of this sandstone is described in Section 3.3.2. The porosity of the sandstone is measured to 12 - 19 % and the permeability is measured to $5 \times 10^{-16} m^2$ [Booij et al., 1998], which is high compared to the surrounding sandstones. Despite of this, fractures are the main groundwater flow channels in the rock [Haldorsen et al., 1996]. During the mining periods, a large amount of pore water was observed in this rock [Booij et al., 1998].

Figure 3.9 show the bedrock profile in Ny-Ålesund, in the direction of the groundwater flow. Figure 3.7 also shows a cross section of the geology in Ny-Ålesund, but in a slightly different direction.

[Booij et al., 1998] did simulations on the groundwater flow in Ny-Ålesund. Figure 3.10 shows the area of the simulation. The simulation was done by assuming recharge only from the base of Vestre Lovenbreen. In Figure 3.10 the supposed lower permafrost boundary are represented as the dotted line.

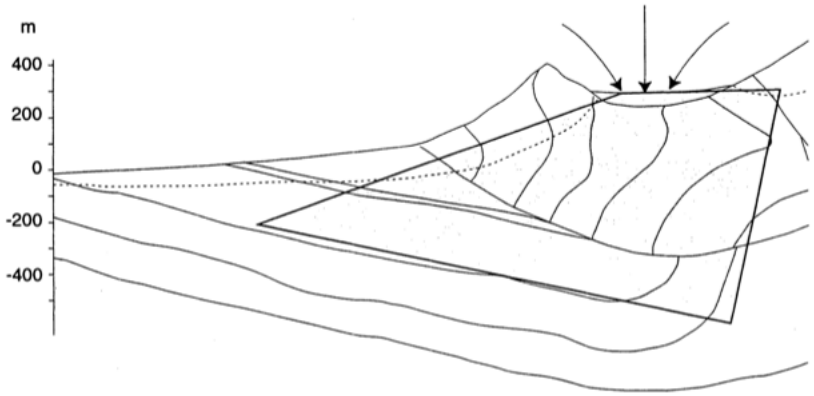

Figure 3.10: *Simulation area [Booij* et al.*, 1998]*

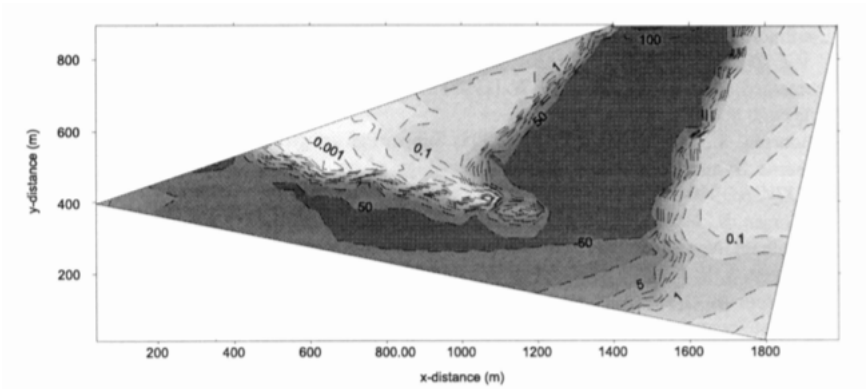

Figure 3.11: *Velocity of groundwater [Booij* et al.*, 1998]*

Figure 3.11 shows the simulated velocity of the groundwater. The velocity of the groundwater is highest in the Permian sandstone, number 11 in Figure 3.7, where the permeability is higher than the surrounding rocks. The velocity of the groundwater are dependent on the water recharge and the permeability of the rocks. In a period with low recharge, the velocity of the groundwater is simulated to vary between 10 m/year and 30 m/year, while in a period with high recharge, the velocity of the groundwater can vary between 30 m/year and 100 m/year [Booij et al., 1998].

Chapter 4

Geothermal Energy in Ny-Ålesund

4.1 Renewable resources in Ny-Ålesund

The Norwegian government and NySMAC have a goal that the environment in Ny-Ålesund should be pristine, and that the human impact on the environment should be kept at a minimum. It is also a goal that the energy production in Ny-Ålesund should be renewable [Sander et al., 2006]. Because of this, it is desirable to replace the current diesel generator for electricity production. The electricity used for heating purposes can be substituted by geothermal energy, reducing the electricity demand. The diesel generator also produces excess heat, that is distributed in a district heating system. The geothermal system must also replace this heat production. Other renewable energy sources must be installed to cover the remaining electricity demand.

4.1.1 Electricity production

Solar energy was considered in [Jørgensen and Bugge, 2009] as a possible renewable energy source that could be installed in Ny-Ålesund. The incoming solar radiation in Ny-Ålesund are low, because of the poor solar radiation on this latitude (discussed in Section 2.1.3). Because of this, even the most efficient solar power plant will only be able to reach a production capacity of 50 kW [Jørgensen and Bugge, 2009]. A solar power plant will maximum produce $50000 - 60000 kWh/year$, and this is only 1 - 2 % of the total demand of electrical energy in Ny-Ålesund. A solar energy power plant in Ny-Ålesund

is therefore evaluated as not suitable [Jørgensen and Bugge, 2009].

Wind energy was also considered in [Jørgensen and Bugge, 2009]. The wind velocity varies between $4.8 - 6.36 m/s$ in different locations in Ny-Ålesund, and based on this, a wind power plant with capacity of maximum 800 kW can be installed [Jørgensen and Bugge, 2009]. The maximum energy production is estimated to $2.2 MWh/year$, and this will form a considerable part of the electric energy demand in Ny-Ålesund. Because of the uncertainty with the complex topography in the area, and high costs, wind energy is evaluated as complicated [Jørgensen and Bugge, 2009].

A deep geothermal system, as discussed in Section 2.3.4, would have been a good opportunity for substituting the present diesel generators for electricity production. There is no deep geothermal system in Norway, and Svalbard might be a good location for a pilot project. In Ny-Ålesund, the geology is known down to about 500 meters, but below this depth there is uncertainties about the geology conditions. On Svalbard there is also challenges with the permafrost and it's vulnerable environment. A deep geothermal system that produces electricity in Ny-Ålesund, can potentially replace the current diesel generators, and make the energy production in Ny-Ålesund renewable.

4.1.2 District heating

Bioenergy is evaluated as a possible replacement for the oil boiler in Ny-Ålesund. Bioenergy can be used for heating purposes and it can be included in the existing district heating system, shown in Figure 3.1. The use of bioenergy involves unwanted air pollution, and is therefore not desired in Ny-Ålesund [Jørgensen and Bugge, 2009].

Geothermal energy is another possibility for making Ny-Ålesund renewable. A geothermal system will not dominate the landscape in the same way as a wind mill or a solar power plant. The different alternatives for geothermal energy are discussed in Section 2.3.1. A shallow geothermal system in Ny-Ålesund can deliver warm water for heating purposes, and can potentially replace electrical heating. A shallow geothermal system can be installed in several different ways, discussed in Section 2.3.3.

Because of the cold climate in Ny-Ålesund, a horizontal geothermal system or a geothermal lake system (discussed in Section 2.3.3) is not possible. The permafrost denies a horizontal system, and the lakes in the area around Ny-Ålesund are all too small. An alternative is a system that utilizes heat from the seawater in Kongsfjorden. The depth of the ice cover in Kongsfjorden during the year need to be known to ensure that the geothermal system does not freeze during the winter season. The seabed in Kongsfjorden also need

to be known in order to find a good location for the pipes. With solution where the geothermal system is located in Kongsfjorden, the challenges with permafrost is not a problem. The temperature in the ocean below the ice cover is relatively stable during the year, and therefore such a system can deliver a stable load of heat.

Groundwater conditions in Ny-Ålesund are discussed in Section 3.3.3. In 1993 and 1994 there was observed a discharge in one of the old coal mines with a flow rate of 11.5 liters per second [Haldorsen et al., 1996]. The temperature of the groundwater below the permafrost is about $3°C$ [Haldorsen and Lautitzen, 1993]. The outflow of groundwater is caused by human activity, and the groundwater discharge is higher than it normally would have been without human activity. A groundwater system based on the discharge could have been an opportunity in Ny-Ålesund, but the outflow of groundwater today is too uncertain.

A vertical geothermal system with the use of a ground source heat pump is the most common on the Norwegian mainland [Midttømme et al., 2010]. The existing knowledge about the technology makes it easier to install a vertical geothermal system in Ny-Ålesund. The geology in the area around Ny-Ålesund, described in Section 3.3.2, is suitable for a shallow geothermal system, and the groundwater flow in the area, described in Section 3.3.3, can provide additional heat to the geothermal system. Simulations of a vertical geothermal system was done by COMSOL Multiphysics to investigate the potential for a vertical geothermal system in Ny-Ålesund.

4.2 COMSOL Multiphysics simulations of a shallow geothermal system

COMSOL Multiphysics is a software platform for solving partial differential equations using the finite element method. COMSOL allows for simulations and analysis of complex models with multiple physics involved [Comsol, 2013]. COMSOL Multiphysics is build up by several modules. The different modules consists of the most important differential equations linked to the physics that the module are based on. One big advantage with COMSOL Multiphysics is that it is easy to do simulations across different physical interfaces. A large material library is included in the program, and it integrates well with several other programs, for example MATLAB. How COMSOL Multiphysics determines it's equations ans solutions, is not considered in this thesis.

The simulations of the geothermal system in this thesis uses the three mod-

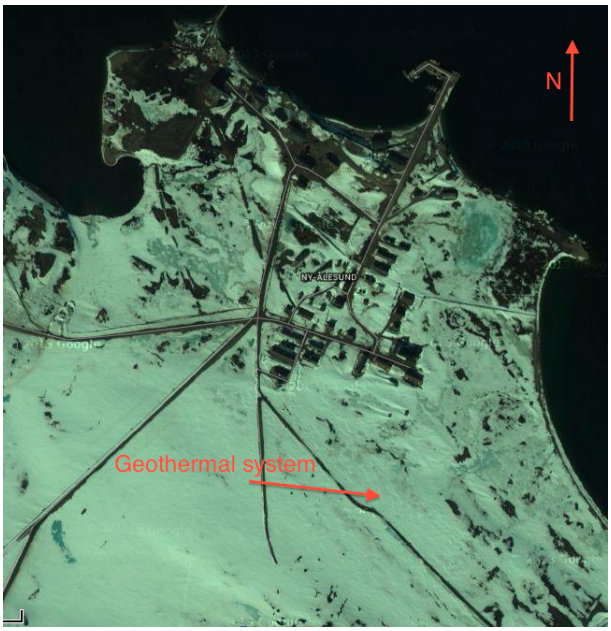

Figure 4.1: *Location of geothermal system. From Google Maps 08.12.2013*

ules 'Heat transfer in porous media', 'Non-isothermal pipe flow' and 'Darcy's law'. The heat transfer module provides tools for heat transfer by conduction, convection and radiation, and well the ability to couple these physics. The pipe flow module is used for simulating the flow of a fluid through a pipe. The pipe flow module provides plots that shows the temperature of the fluid in the pipe, as well as the velocity and pressure of the fluid. Darcy's law was also included in the model for describe the groundwater flow. This module provides the opportunity to describe fluid flow through a porous media.

COMSOL Multiphysics was used to simulate a shallow geothermal system in Ny-Ålesund. The goal of the simulation was to see the potential for a geothermal system and the influence on the temperature in the ground around the geothermal pipe. Particularly, it was interesting to see the changes in the permafrost, as well as the groundwater flow influence on the effect of the geothermal system.

4.2.1 Model parameters

The geometry of the model is shown in Figure 4.2. The geometry is 200 × 200 × 200 m, and the origin, (x,y,z) = (0,0,0), is located in the center of the top surface. Simulations has been done to ensure that the size of the

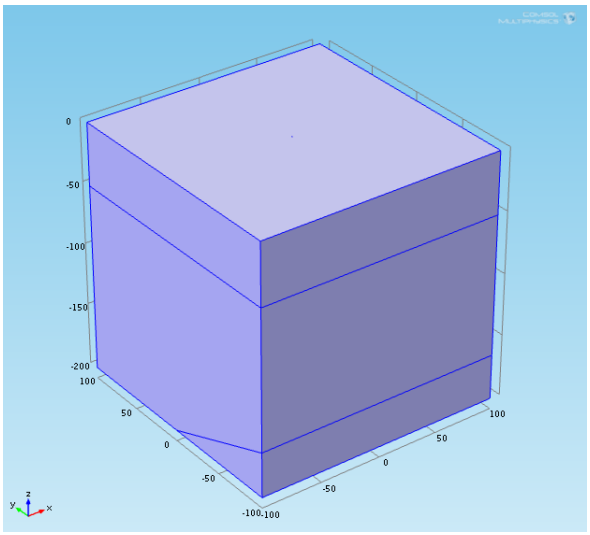

Figure 4.2: *Geometry of the model in COMSOL Multiphysics*

geometry is big enough. When the geometry is defined as $200 \times 200 \times 200$, the sides of the cubes are not effected by the geothermal system.

The model simulates a geothermal system located approximately as shown in Figure 4.1, just south of the settlement of Ny-Ålesund. The geothermal system is located along the cross section C - C' in Figure 3.7, in the middle of the Kapp Starostin Formation, rock number 11 in Figure 3.6. The model also includes the Gipshuken Formation, number 12 in Figure 3.6, which has a dip of 20° [Hjelle et al., 1999]. The Gipshuken Formation is only present in one of the corners of the model geometry. The model geometry is oriented parallel to the boundary between the Kapp Starostin Formation and the Gipshuken Formation. In Figure 4.2 the y-coordinate has the same direction as the dip of the Gipshuken Formation.

The geological conditions in Ny-Ålesund are described in Section 3.3.2. The physical properties of the geology that are included in the model are summarised in Table 4.1. Note that the dynamic viscosity, permeability and porosity of the Gipshuken Formation does not effect the model, as the groundwater flow are chosen to only appear in the Kapp Starostin Formation. This is detailed in a later paragraph. The dynamic viscosity, permeability and porosity does not effect the other parts of the simulation.

Because of the high heat capacity of water ($4186 Jkg^{-1}K^{-1}$) the heat capacity in the rock is strongly dependent on its water content. In a porous rock, the heat capacity must be adjusted because of the water content by

	Kapp Starostin	Gipshuken
Thermal conductivity $[Wm^{-1}K^{-1}]$	3.0	2.4
Density $[kgm^{-3}]$	2700	2700
Heat capacity $[JL^{-1}K^{-1}]$	1350.4	1050.16
Dynamic viscosity $[Pas]$	1.28×10^{-6}	1.4×10^{-6}
Permeability $[m^2]$	5×10^{-11}	6×10^{-13}
Porosity [%]	15	6

Table 4.1: *Physical properties of the Kapp Starostin Formation and the Gipshuken Formation [Booij* et al.*, 1998, Clauser and Huenges, 1995, Banks, 2012] [Kirsti Midttømme, pers.comm. 2013]*

using the following formula [Kirsti Midttømme, pers.comm. 2013]

$$C_p = C(1-p) + 4186 \times p \tag{4.1}$$

where C_p is the heat capacity of the porous rock, C is the heat capacity of the rock and p is the porosity of the rock.

Both the Gipshuken Formation and the Kapp Starostin Formation contains rocks with an estimated heat capacity of $850JL^{-1}K^{-1}$ [Kirsti Midttømme, pers.comm. 2013]. For the Kapp Starostin Formation, with a porosity of 15%, the heat capacity is calculated to $1350.4JL^{-1}K^{-1}$. The Gipshuken Formation, with a porosity of 6%, the heat capacity is calculated to $1050.16JL^{-1}K^{-1}$.

A geothermal system is included in the center of the geometry, from (x,y,z) = (0,0,0) to (x,y,z) = (0,0,-100). The geothermal system consists of a single U-tube with a depth of 100 m. The pipe in the geothermal system is a 0.0015 mm thick tube made of thermoplastics. The geothermal fluid is chosen to be water with a mix of propylene glycol, in a concentration of 32.9% [Banks, 2012]. This fluid has a freezing point of $-15°C$ which makes it well suitable for a geothermal system in cold climates. Propylene glycol also have low toxicity. The physical properties of propylene glycol mixture are summarized in Table 4.2. In the model, the inlet water in the geothermal system was set to have a temperature of $-10°C$.

To ensure transient turbulent flow in the pipe, the Reynold's number must be grater than 2500. This is discussed in Section 2.1.2. For a pipe with 40 mm outer diameter, the flow rate in the pipe must be minimum 31 liters per minute to make sure that the flow is turbulent [Banks, 2012]. For propylene glycol mixture, with a density of $1035kgm^{-3}$, this corresponds to a flow rate of 0.534 kg per second, which is the flow rate of the simulated geothermal system.

In the model, a permafrost zone is defined in the upper 50 meters [Booij et al., 1998, Haldorsen et al., 1996]. The temperature gradient in the area are assumed

Propylene glycol mixture	
Concentration [%]	32.9
Freezing point [$°C$]	-15
Density [kgm^{-3}]	1035
Heat capacity [$JL^{-1}K^{-1}$]	3884
Thermal conductivity [$Wm^{-1}K^{-1}$]	0.417
Dynamic viscosity [cP]	8.32

Table 4.2: *Physical properties of propylene glycol mixture [Banks, 2012]*

to be 1.6°C per 100 m [Haldorsen and Lautitzen, 1993]. The geothermal gradient is included in the model as a temperature difference between the base and the lower permafrost limit. The temperature of the permafrost layer is set to an initial value of 0°C. The temperature at the plane between the permafrost and the Kapp Starostin layer, at z = -50, are set to a constant value of 0°C. This is done to ensure permafrost conditions in the upper 50 meters. The temperature of the plane at the base of the geometry, at z = -200, are set to a constant value of 3.2°C. This is done to maintain the geothermal gradient during the simulations. The temperature difference between the lower permafrost limit and the base of the geometry, is equivalent to a geothermal gradient of 1.6°C per 100 m.

The groundwater flow is also included in the model. Originating from Bøggerbreen and Lovenbreen, the main direction of the groundwater flow in the area around Ny-Ålesund is towards the Easter mine, which is the main discharge point. The groundwater flow is described in Section 3.3.3. Figure 3.11 shows that there is a groundwater flow beneath the Easter mine that continues towards the sea. The groundwater flow in the model is, from Figure 3.11, assumed to be around 10 meters per year in the Kapp Starostin layer, rock number 11 in Figure 3.6. In the geometry of the model, Figure 4.2, the groundwater flow is in negative y-direction, which is towards the sea. The groundwater flow is assumed to be time independent, and also constant during the whole simulation period.

To see the long term effects on the temperature in the ground with a geothermal system installed, the simulations span a 30 year period. Calculations done by [Banks, 2012] shows that, for a geothermal system similar to the done described here, 30 years is needed for the temperature to stabilize.

To illustrate the results of the simulation, the temperature distribution is shown along three cut planes. Figure 4.3 shows the surface of the geometry, a xy-plate with z = 0. Figure 4.4 shows the slice of the yz-plane at the center of the cube. Note that the plots along the plane in Figure 4.4 have different axes than the model geometry in Figure 4.2, with origin in the left

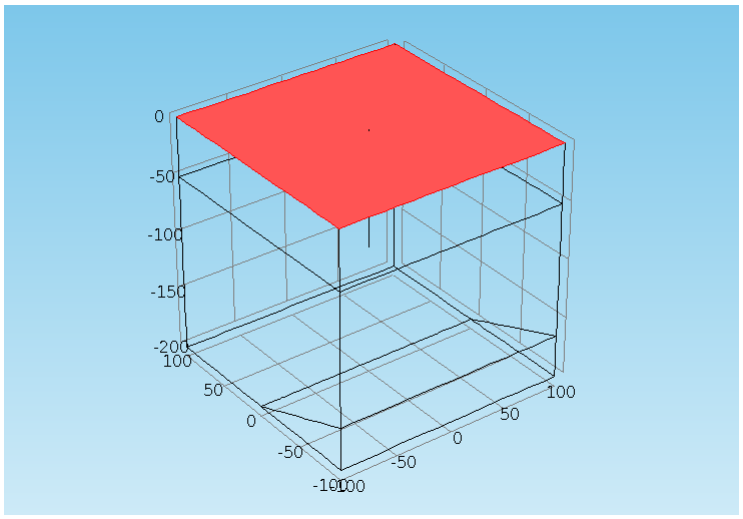

Figure 4.3: *Cut plane on the surface used to show results of the simulations*

hand corner. Figure 4.5 shows a xy-plane at a depth of z = -65 meters.

4.2.2 Assumptions and limitations to the model

Permafrost and latent heat

The constant temperature of $0°C$ at a depth of 50 m is not natural. This simplification was done to be able to see the change in the permafrost zone when the geothermal system was installed. A consequence of having a constant temperature at this depth, is that the temperature distribution of the ground in the simulations will have an unnatural discontinuity at a depth of 50 m.

The depth of the permafrost zone is set to be constant in the area of the simulation. In reality, the permafrost will most likely have small variations. Also, the variations in the air temperature is not taken into account in the model. The temperature variations in the ground, caused by the changing air temperature, effects the upper 10 meters [Banks, 2012]. If the variations in the air temperature was included in the model, the permafrost layer would have been effected by the increasing temperature, and the upper permafrost would have melted in the summer season. If this was included in the model, latent heat (described in Section 2.1.1) from the phase transformations from ice to water could have influenced the effect on the geothermal system.

Latent heat is not taken into account in the model. Latent heat is the

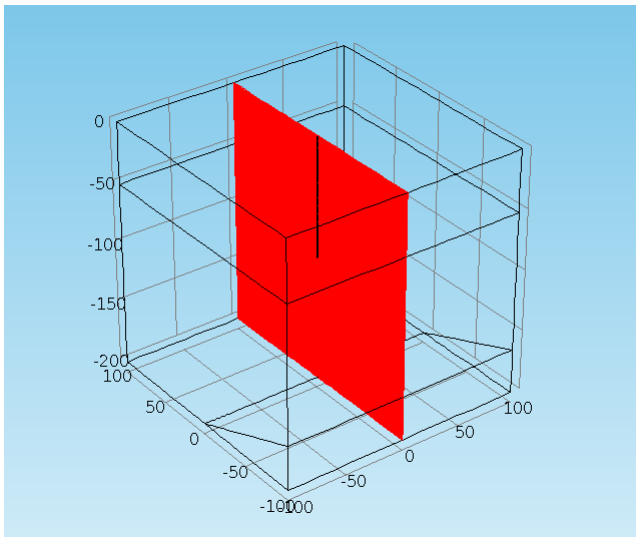

Figure 4.4: *Cut plane used to show results of the simulations*

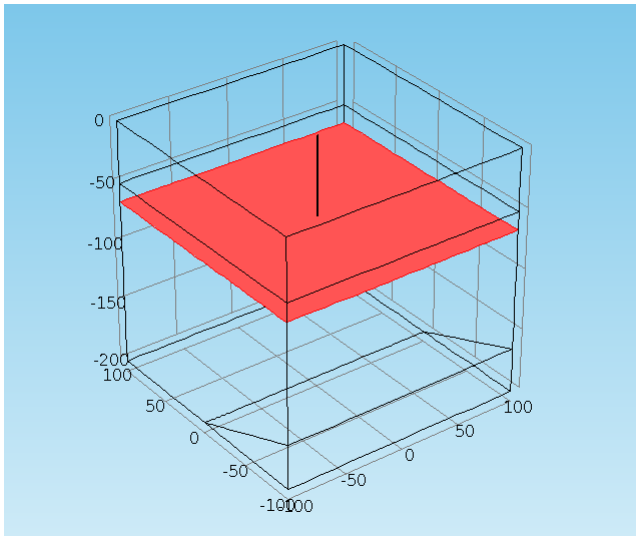

Figure 4.5: *Cut plane at a depth of 65 meter used to show results of the simulations*

amount of energy required to make a material undergo a phase transformation, as described in Section 2.1.1. The geothermal pipe will cool down the subsurface, and increase the permafrost depth around the pipe. The area around the geothermal pipe, that initially has temperature above freezing, but freezes because of the geothermal system, would have been effected if latent heat were included in the model. With latent heat included in the model, the temperature in the subsurface would have been higher than without latent heat included. This is because of the additional energy required to undergo a phase transformation from water to ice. The temperature around the pipe decreases linearly with time when latent heat is not included. Because of difficulties with including latent heat in the model in COMSOL Multiphysics, and the minor influence on the effect of the geothermal system, latent heat is chosen to be neglected.

Geological parameters and groundwater flow

Most of the geological parameters in Table 4.1 are based on rocks with same properties as the rocks in Ny-Ålesund. In the model, the rocks are assumed to be homogeneous.

The groundwater is assumed to be constant during the whole year, with a flow of 10 meters per year. This is based on results from [Booij et al., 1998]. The groundwater flow is also assumed to only flow in one direction. These simplifications are done to be able to include the groundwater flow in the model. Groundwater flow has a large influence on the heat transport in the ground, and therefore can cause an increasing in the effect on the geothermal system. In reality, the groundwater flow will vary in depth and will not be constant during the year. It will most likely increase in summer, when the glaciers are melting, and decrease in winter [Haldorsen and Lautitzen, 1993].

4.3 Results

The results of the simulations are separated into two parts, with and without groundwater flow included in the model. This is done to illustrate the effect of the groundwater flow on the temperature distribution in the ground and delivered energy from the geothermal system.

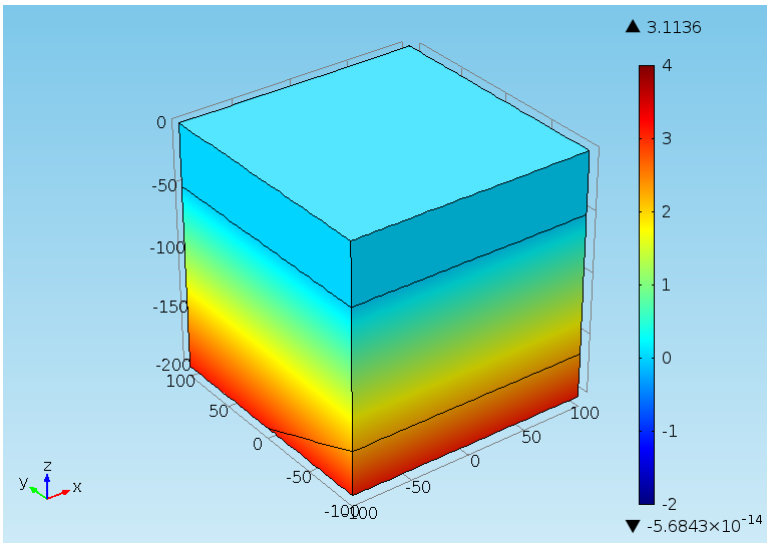

Figure 4.6: *Initial temperature distribution in the geometry without groundwater flow. Used for initial conditions in the simulations*

4.3.1 Simulations without groundwater included in the model

Figure 4.6 shows the temperature distribution in the model geometry after a stationary simulation with the initial conditions described in Section 4.2.1. The stationary temperature distribution along the cut plane in Figure 4.4 is shown in Figure 4.7. This temperature distribution is used as initial condition in the simulations. As described in Section 4.2.1, the upper 50 meters are permafrost, and below this the geothermal gradient is $1.6°C$ per 100 m. The temperature is distributed linearly from the base to the lower permafrost layer in Figure 4.7. The temperature scale in this figure, and all the following figures, are in Celsius. Note that the temperature scale also contains information about the highest and lowest temperatures in the plot. The value of the highest temperature is in the top of the scale, and the lowest at the bottom of the scale.

Figure 4.8 shows the temperature distribution in the ground without groundwater flow after 30 years of simulation. The temperature distribution around the pipe is symmetric, and the cooling effect from the geothermal system is evenly distributed in the ground. The discontinuity in the temperature at a depth of 50 m is caused by the constant temperature set at this depth, as discussed in Section 4.2.2. The physical characteristics of the Kapp Starostin Formation and the Gipshuken Formation, described in Section 4.2.1, are too similar to have an effect on the temperature distribution. The decreasing temperature around the pipe causes a change in the permafrost, and

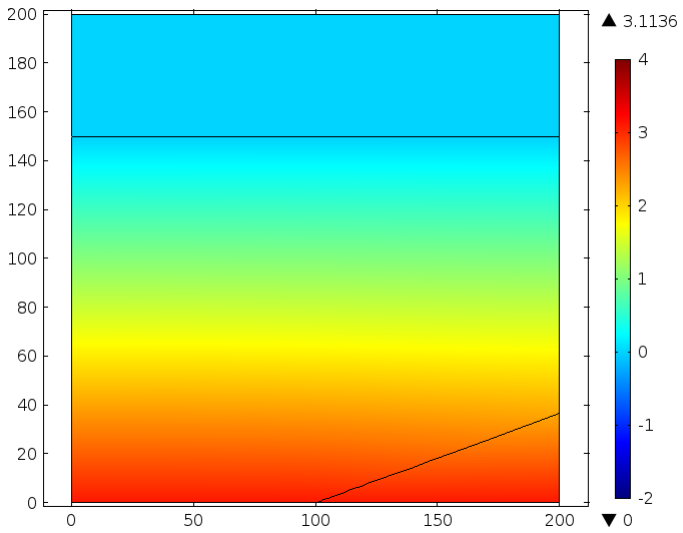

Figure 4.7: *Initial temperature distribution along the cut plane in Figure 4.4 without groundwater flow*

therefore the permafrost depth is increased around the pipe.

The temperature on the surface, along the plane in Figure 4.3, after 30 years of simulation with no groundwater flow is shown in Figure 4.9 and Figure 4.10. The initial temperature on the surface was set to $0°C$. From Figure 4.9, the temperature on the surface after 30 years are in the range of $-0.16°C$ to $-1.62°C$. The highest temperature on the surface after the simulation, $-0.16°C$, is lower than the initial temperature, $0°C$. This indicates that the geothermal system has cooled the whole surface, and increased the permafrost. Figure 4.10 shows the temperature on the surface, with contour lines included. Note that this plot have different axes than Figure 4.9 to illustrate the temperature around the geothermal pipe. The contour lines shows that in a circle with radius 20 m around the geothermal pipe, the temperature have decreased with $0.5°C$.

Figure 4.11 shows the output temperature of the geothermal fluid. The input temperature of the fluid was $-10°C$, and the temperature difference of the input and output water is approximately $8.52°C$. The figure also shows that the temperature of the geothermal fluid is decreasing over time, but in this simulation, the fall in temperature very small. The decreasing temperature of the output water is caused by the cooling of the ground, as the cold circulating fluid in the pipes cools the ground. Based on the temperature difference, the effect of the geothermal system is calculated. The effect of the system over 30 years are also shown in Figure 4.11. The simulated effect of the geothermal is approximately 18 kW.

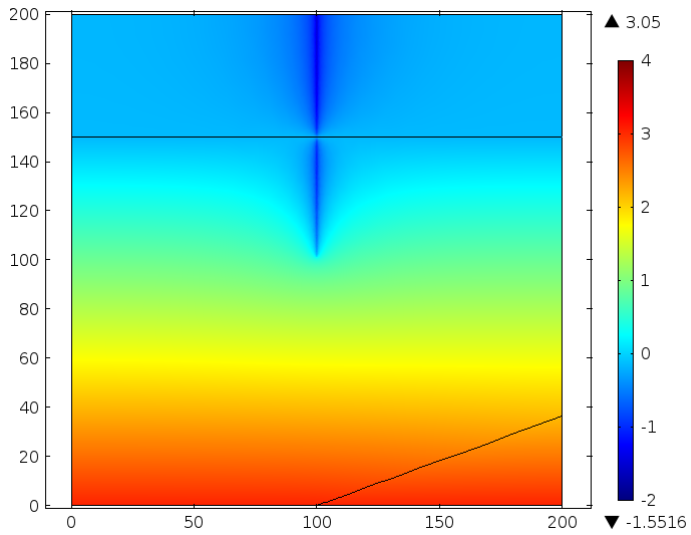

Figure 4.8: *Temperature distribution along plane in Figure 4.4 after 30 years of simulation without groundwater flow*

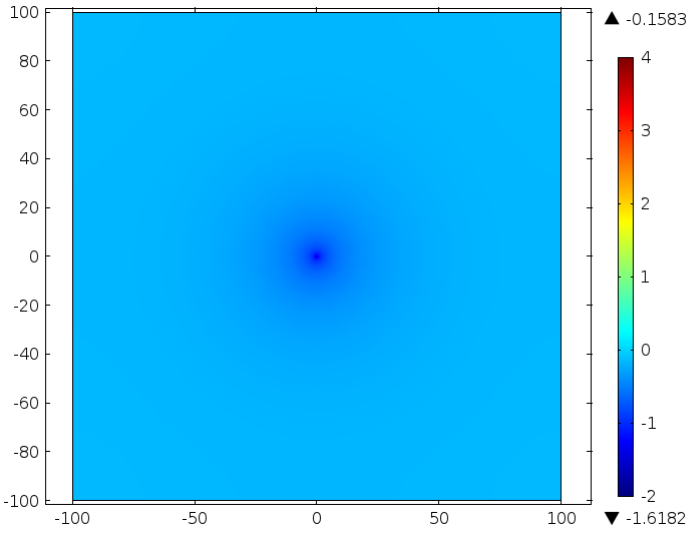

Figure 4.9: *Temperature on the surface after 30 years of simulation with no groundwater flow*

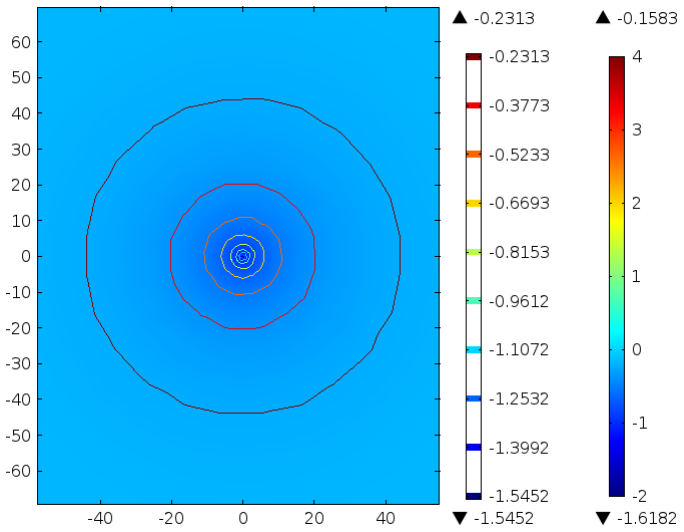

Figure 4.10: *Temperature on the surface, with contours, after 30 years of simulation with no groundwater flow*

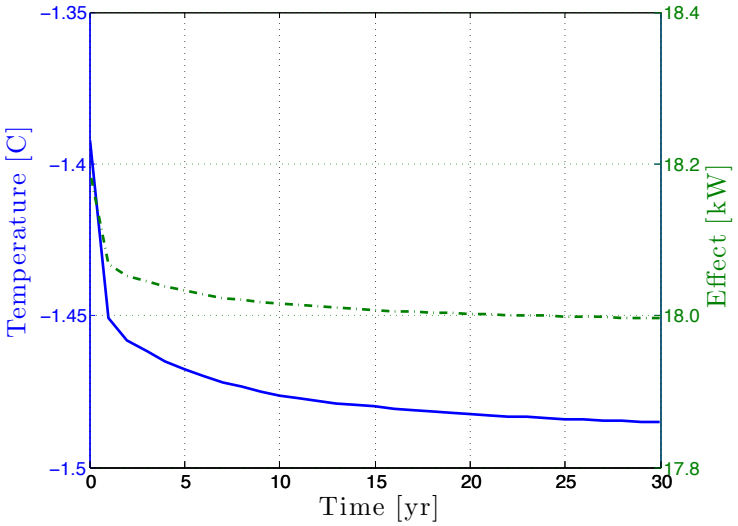

Figure 4.11: *Output temperature and effect of the geothermal system without groundwater*

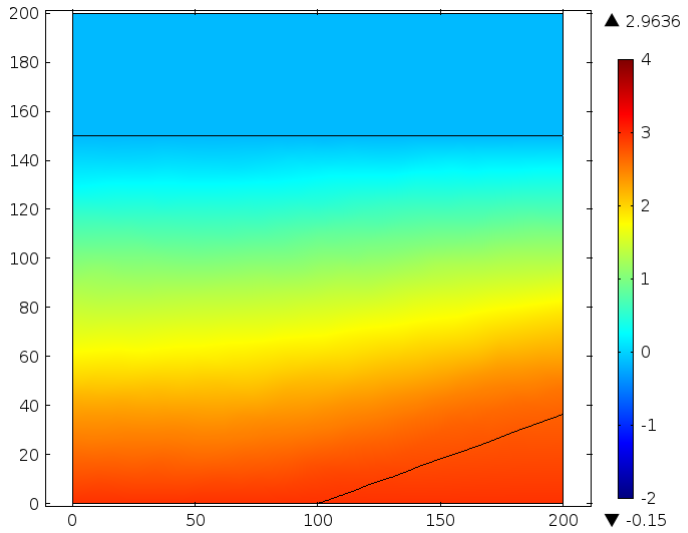

Figure 4.12: *Temperature distribution along the cut plane in Figure 4.4 when the groundwater flow is included*

4.3.2 Simulations with groundwater included in the model

The natural conditions in Ny-Ålesund will involve groundwater flow. Figure 4.12 shows the temperature distribution of a stationary simulation, along the cut plane in Figure 4.4, when groundwater flow is included. This figure shows the natural temperature distribution in the ground before a geothermal system is installed. Comparing Figure 4.7 and Figure 4.12, the groundwater influence on the temperature distribution is clear. The groundwater flow in the Kapp Starostin Formation, in negative y-direction, forces the heat above the Gipshuken Formation and creates an increased temperature here.

Figure 4.13 (along the cut plane in Figure 4.4) shows the temperature distribution in the ground and around the geothermal system with the influence of groundwater flow. The geothermal system creates a zone of depressed temperature around the borehole. The groundwater flow provides an extra heat source to the geothermal system, in addition to the geothermal heat flux. The temperature around the geothermal well is increased compared with no groundwater flow. In addition, the shape of the temperature front around the well is not symmetric. In the direction of the groundwater flow, the temperature in the ground decreases after passing the geothermal well, and in front of the geothermal system, the temperature is increased. In the permafrost zone (the upper 50 meters) the temperature distribution is still symmetric since there is no groundwater flow here. The temperature in the

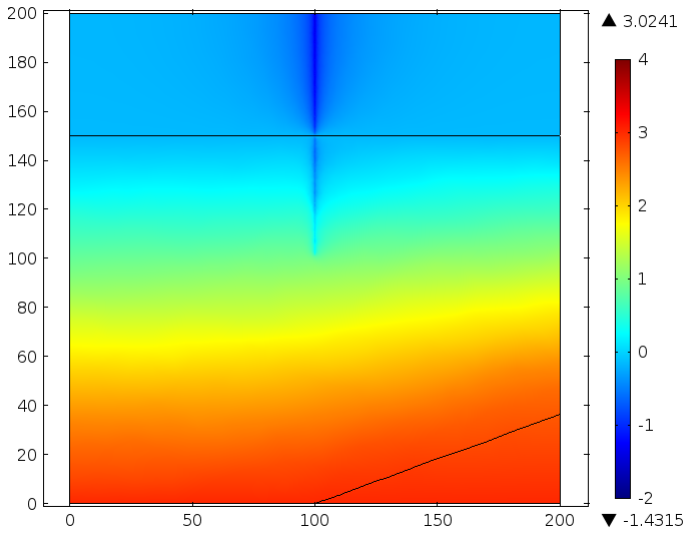

Figure 4.13: *Temperature distribution of stationary solution along the cut plane in Figure 4.4 with geothermal system and groundwater included*

Kapp Starostin Formation is also increased above the Gipshuken Formation caused by the groundwater flow.

Figure 4.14 shows the temperature distribution in the ground with groundwater flow after 30 years of simulation along the cut plane in Figure 4.4. Just as in Figure 4.13, the temperature distribution around the geothermal pipe is affected by the groundwater flow. The temperature is also increased above the Gipshuken Formation caused by the groundwater flow. Figure 4.14 and Figure 4.13 are similar because the time dependent solution stabilizes after a short period of time. The reason for this is the constant temperature at the base of the permafrost layer and at the base of the geometry, and also since the stationary solution is used as the initial value for the time dependent simulation.

Since there is no groundwater flow in the permafrost layer, the temperature on the surface show minor differences compared to the results in the simulation with no groundwater flow. The temperature on the surface along the cut plane in Figure 4.3, with the groundwater flow included, is shown in Figure 4.15. Comparing the results shown in Figure 4.15 and Figure 4.9, the temperature distribution are equivalent. The temperature below the permafrost layer, within the Kapp Starostin Formation, will be effected by the groundwater flow.

Figure 4.16 and Figure 4.17 shows the temperature distribution at a depth of 65 meters, along the plane in Figure 4.5. In both figures, contour lines are

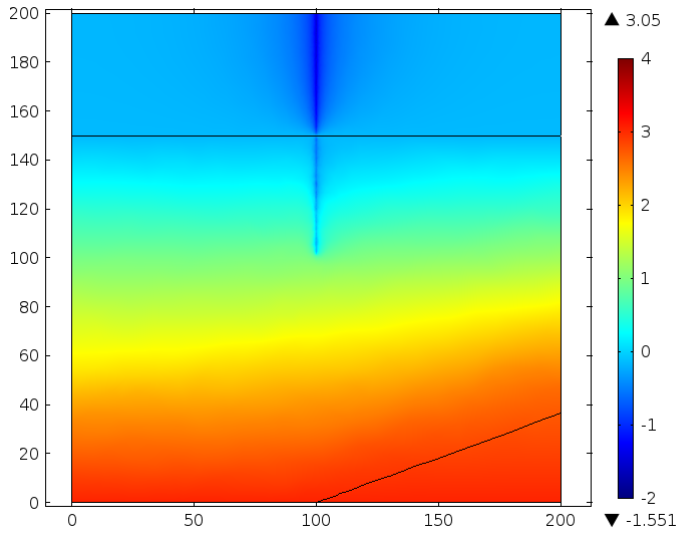

Figure 4.14: *Temperature distribution after 30 years of simulation with groundwater flow included*

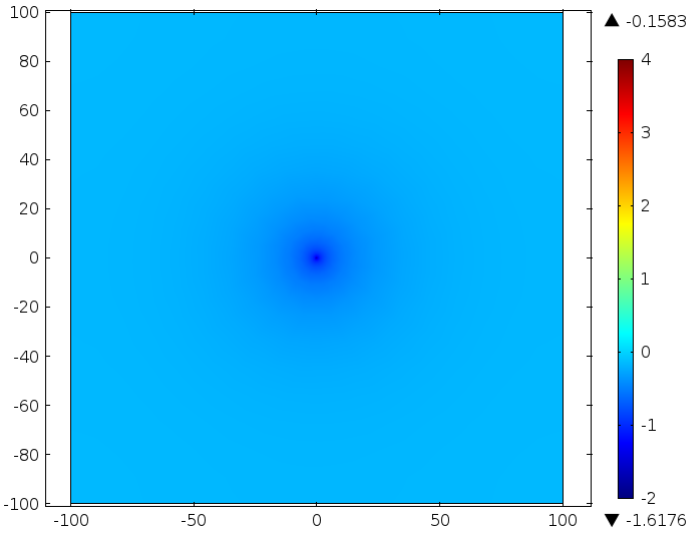

Figure 4.15: *Temperature on the surface after 30 years with groundwater flow included in the model*

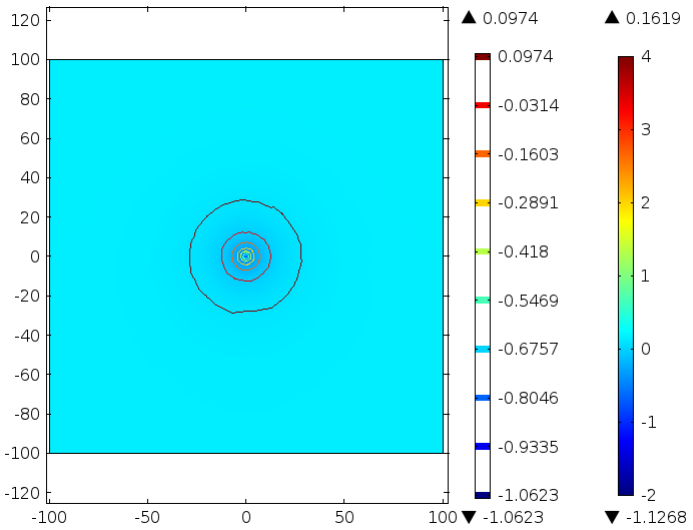

Figure 4.16: *Temperature along the cut plane in Figure 4.5 without groundwater included*

included to easily see the temperature distribution along the plane. Note that the temperature scale on the contours are not the same in the two figures. The cooling effect on the ground in Figure 4.16 are evenly distributed around the geothermal pipe. In contrast, the temperature distribution in Figure 4.17, the groundwater flow effects the temperature, and makes a complex temperature distribution. The direction of the groundwater flow in negative y-direction can also be seen in Figure 4.17. When the groundwater flows through the geothermal pipe, it makes an area with increased temperature in front of the geothermal pipe. Behind the geothermal system, the groundwater flow creates a zone of decreased temperature.

The temperature of the water entering the geothermal system was set to $-10°C$. The output temperature of the water from the geothermal system over 30 years are shown in Figure 4.18. The temperature difference between the input and output water in the geothermal system is approximately $8.52°C$. This is the same result as when the groundwater was not included. The temperature of the output water decreases the first years of simulation, before stabilizing after about 10 years.

Figure 4.18 also shows the effect of the geothermal system from the difference between the temperature of the input and output water. This result is also the same as when the groundwater was not included. The simulated effect of the geothermal system is approximately 18 kW.

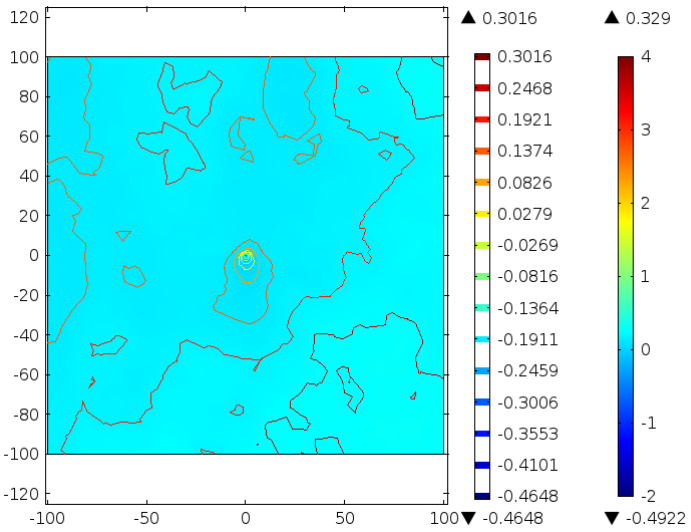

Figure 4.17: *Temperature along the cut plane in Figure 4.5 with groundwater included*

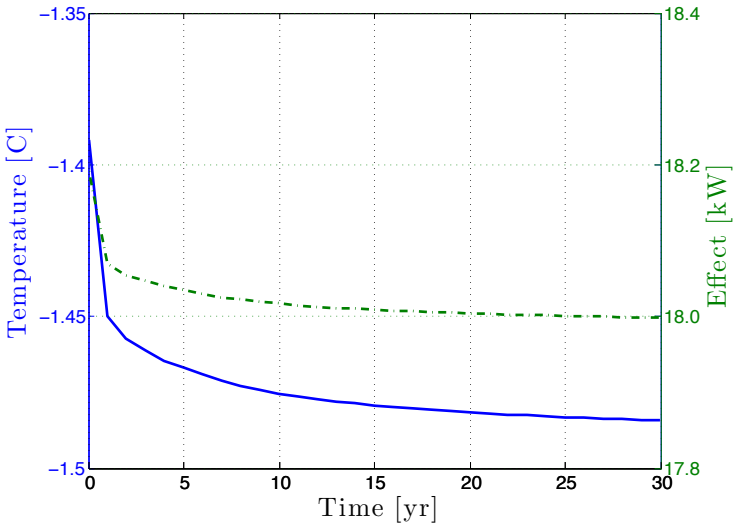

Figure 4.18: *Output temperature and effect of the geothermal system with groundwater*

4.4 The potential of the geothermal system

Figure 4.11 and Figure 4.18 shows that the temperature of the output water from the geothermal system are approximately $-1.48°C$. The temperature difference between the input water, with a temperature of $-10°C$, is then $8.52°C$. This temperature difference gives, from Figure 4.18, approximately G = 18kW heat extracted from the ground.

A heat pump can lift the temperature, and increase the effect of the geothermal system, as discussed in Section 2.3.2. The total heating effect, H, can be calculated by combining Equation 2.24 and Equation 2.25. If we assume that the heat pump has a $COP_H = 4$ [Banks, 2012], the total heating effect, from the ground and the heat pump combined, can be calculated as

$$H = \frac{G}{1 - \frac{1}{COP_H}} = 24kW \tag{4.2}$$

The total heating effect of 24 kW is provided that there is an electricity supply to power the heat pump with effect of

$$E = H - G = 6kW \tag{4.3}$$

The energy production and consumption in Ny-Ålesund are described in Section 3.1.2. From Table 3.1, the total energy consumed by heating purposes in 2005 was 4.8GWh [Jørgensen and Bugge, 2009]. Given an even distribution of heat consumption, and that a geothermal system has a total heating effect of 24kW, this translates to 23 such systems. But since the heating demand varies with the seasons, and even during the day, this amount of systems is not able to produce enough heat during peak consumption. From Table 3.1, the energy system in Ny-Ålesund today has a maximum capacity of 1200 kW dedicated to heating. This means that 50 such systems are needed in order to match the current heat production capacity in Ny-Ålesund.

Even though the average amount of geothermal systems needed during the year is 23, 50 geothermal systems are needed to cover peak consumption. This means that during the warmer seasons, many of the systems will produce potentially wasted energy. In order to remedy this, the temperature of the input water in the geothermal system can be adjusted to modify the effect of the system.

A geothermal system can be installed to cover the heating demand for a single building, but it can also be extended with several geothermal pipes to deliver heating for several buildings. In cold northern climate, the spacing between the boreholes should be more than 4.6 meters apart to achieve that

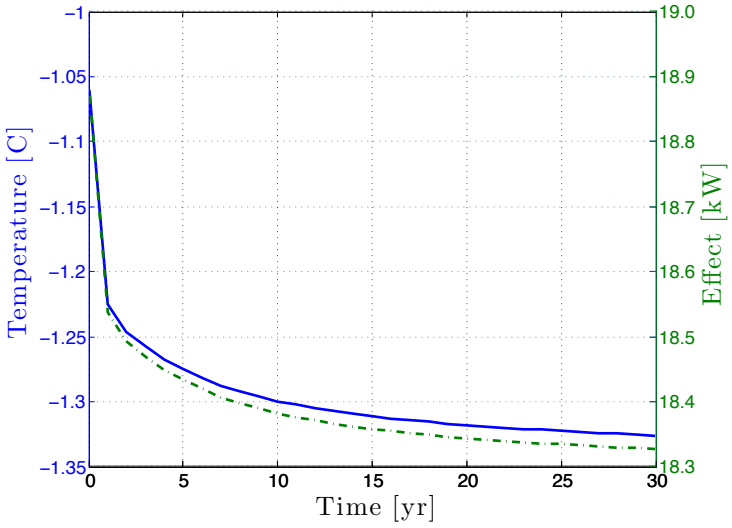

Figure 4.19: *Output of the geothermal system when the geothermal well is 150 m deep*

the boreholes does not have a thermal influence each other [Omer, 2008]. When installing several geothermal wells, it is important to take the groundwater flow into account. As shown in Figure 4.14, the groundwater flow will create a zone of decreased temperature behind the geothermal well. The suggestion of 4.6 meters between the boreholes from [Omer, 2008], may be to little when there is groundwater flow in the area.

4.4.1 Testing model variations

Depth of geothermal well

The depth of the geothermal well will influence the output effect of the system. Figure 4.19 shows the output temperature and the effect of the geothermal system when the depth of the well is increased to 150 m. The groundwater is included in this simulation. Figure 4.19 shows that the temperature difference of the input and the output water will be approximately $8.7°C$, and the output effect will be about 18.3 kW. If a geothermal system should be installed in Ny-Ålesund, the drilling cost must be evaluated. The additional cost of drilling will not necessary be profitable compared to the increased effect.

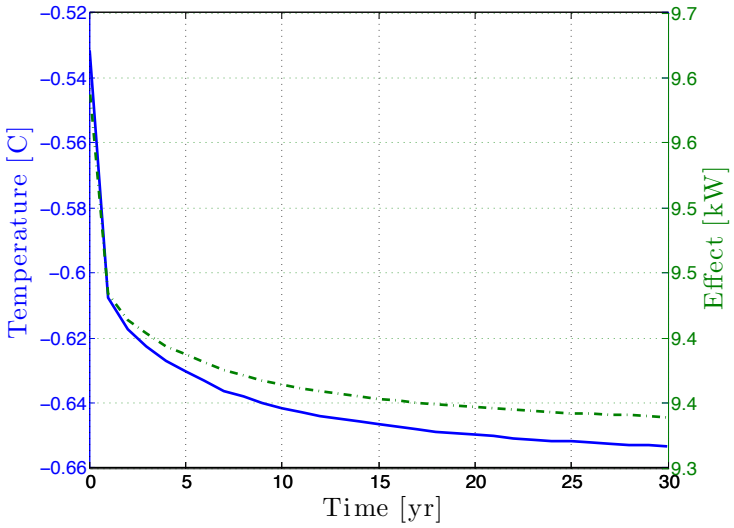

Figure 4.20: *Output of the geothermal system when the input water is* $-5°C$

Temperature of inlet water

The temperature of the input water will also influence on the effect of the geothermal system. Figure 4.20 shows the output temperature and the effect of the geothermal system when the temperature of the input water is set to $-5°C$. Groundwater flow is included in this simulation. The temperature of the output water stabilizes around $-0.65°C$, which corresponds to a temperature difference of $4.35°C$. The simulated effect of the geothermal system is 9.4 kW in this case. Comparing Figure 4.18 and Figure 4.20, shows that the temperature of the inlet water to the geothermal system will have a great influence on the effect of the geothermal system. Figure 4.14 shows that the temperature around the geothermal pipe will decrease, caused by the cold geothermal fluid circulating in the pipes. When the temperature of the geothermal fluid is increased, this decrease in ground temperature will be smaller. Even though the effect of the geothermal system is lower, it is positive that there is smaller influence on the environment.

The temperature in the ground will decrease if the temperature of the input water is decreased. The effect of the geothermal system will be higher, but the cooling of the ground may cause a decreased lifetime of the geothermal system.

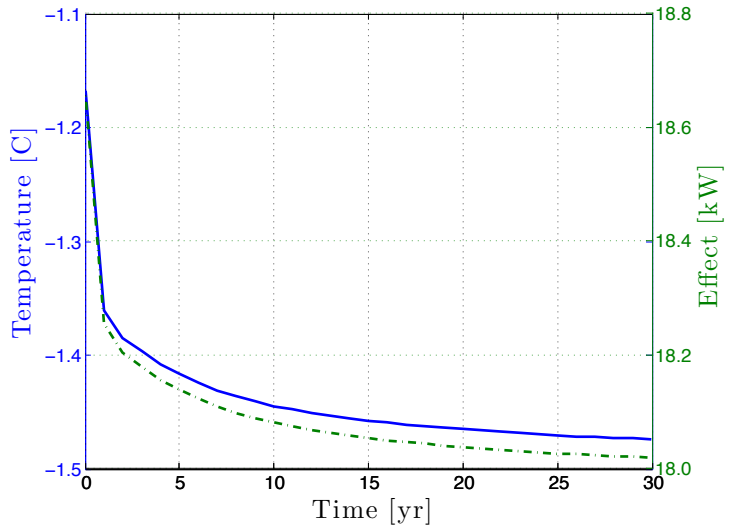

Figure 4.21: *Output of the geothermal system when the groundwater flow is set to 50 m/year*

Groundwater flow

There is some uncertainties about the groundwater conditions in the area where the geothermal system is simulated. The effect of the geothermal system, both with and without groundwater included in the model, are approximately 18kW. The groundwater flow is set to 10 m/year in the model. When the recharge of groundwater is high, the velocity of the groundwater flow can be as high as 100 m/year in some areas in Ny-Ålesund [Booij et al., 1998]. The flow will vary with the seasons, so the constant velocity of 10 m/year represents the lower bar of groundwater flow in the area.

Simulation with groundwater flow set to 50 m/year and 100 m/year was done to test it's influence on the effect on the geothermal system. Figure 4.21 and Figure 4.22 shows the output of the geothermal system when the groundwater flow is set to 50 m/year and 100 m/year respectively.

In both cases the effect of the geothermal system is just above 18kW. Comparing Figure 4.18 with these two figures, the effect of the geothermal system increases with a very small amount when the groundwater flow increases from 10 m/year to 50 m/year and 100 m/year.

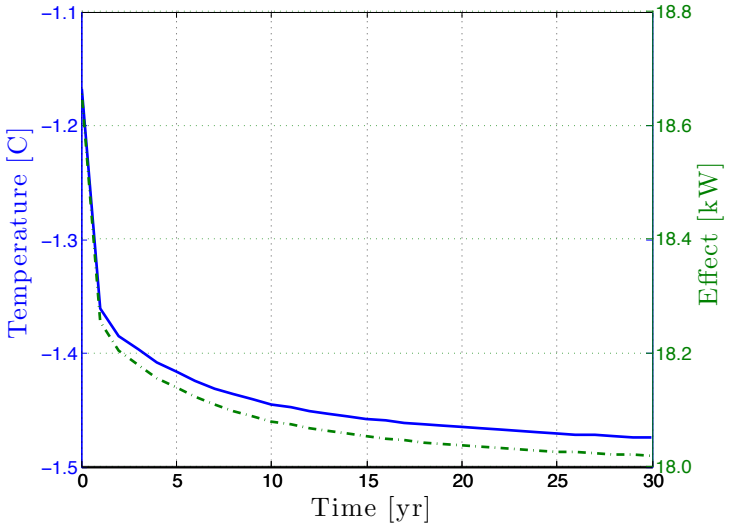

Figure 4.22: *Output of the geothermal system when the groundwater flow is set to 100 m/year*

Chapter 5

Conclusion

The geological conditions in Ny-Ålesund are found to be suitable for a shallow geothermal system. The geothermal gradient and the groundwater flow in the area contributes as important heat sources. A geothermal system can be included in the current district heating system in Ny-Ålesund, replacing heat produced by the diesel generator. This means that a shallow geothermal system can partially replace the current diesel based energy source. This is a step towards the goal of a renewable Ny-Ålesund.

A model of a shallow geothermal system in Ny-Ålesund was made using COMSOL Multiphysics. The geothermal system in the simulations is a single U-tube with a borehole depth of 100 m. The model includes the geological parameters of the rocks in the area, as well as groundwater flow and permafrost conditions.

The simulations indicates the required size of the geothermal system. The result show that such a system should give at least an effect of 18kW. With use of a heat pump with COP = 4, this gives a theoretical net effect of 24kW. To replace the current heat production capacity, approximately 50 geothermal systems are needed.

The simulations shows that a geothermal system will cool down the ground, and the permafrost will increase in the area around the geothermal well. The simulations also shows that the groundwater flow has effect of the temperature distribution around the geothermal pipe.

5.1 Future work

The simulations done in COMSOL Multiphysics have potential for several improvements. As mentioned in Section 4.2.2, some physical aspects has not been considered, such as latent heat and air temperature. Assumptions on groundwater flow and permafrost depth can be made more accurate by field work experiments and measurements. All of these measures will contribute to improve the model and the accuracy of the simulations. Knowledge of the groundwater flow and permafrost conditions in Ny-Ålesund are also important for finding the best location for a geothermal system with several pipes.

Since the diesel generator produces both electricity and heat, if the heating demand is covered by a geothermal system, the electricity demand needs to be covered by another renewable energy source. The heat pumps in a geothermal system also rely on electricity. Knowledge about renewable energy sources working in cold climates are needed to find the best substitute for electricity production.

Deep geothermal energy is an opportunity for electricity production in Ny-Ålesund. Norway does not have any deep geothermal systems today, and Ny-Ålesund can be a good location for a pilot project. Svalbard has higher geothermal gradients than the Norwegian mainland. Replacing the current diesel generator with a deep geothermal system in Ny-Ålesund, will contribute to reduce the negative influence on the environment. A geological survey is needed in order to expose the unknown factors of the geothermal and permafrost conditions. An evaluation of the cost of such a pilot project must also be investigated.

References

[Antics et al., 2013] Antics, M., Bertani, R. and Sanner, B. (2013). Summary of EGC 2013 Country Update Reports on Geothermal Energy in Europe. European Geothermal Congress .

[Bakirci, 2010] Bakirci, K. (2010). Evaluation of the performance of a ground-source heat-pump system with series {GHE} (ground heat exchanger) in the cold climate region. Energy *35*, 3088 – 3096.

[Banks, 2012] Banks, D. (2012). An Introduction to Thermogeology: Ground Source Heating and Cooling. Wiley.

[Barbier, 2002] Barbier, E. (2002). Geothermal energy technology and current status: an overview. Renewable and Sustainable Energy Reviews *6*, 3 – 65.

[Booij et al., 1998] Booij, M., Leijnse, A., Haldorsen, S., Heim, M. and Rueslatten, H. (1998). Subpermafrost Groundwater Modeling in Ny-Ålesund, Svalbard. Nordic hydrology *29*, 385–396.

[Boyle, 2004] Boyle, G. (2004). Renewable Energy 2E. Oxford University Press, Incorporated.

[Clauser and Huenges, 1995] Clauser, C. and Huenges, E. (1995). Thermal conductivity of rocks and minerals. Rock physics and phase relations: a handbook of physical constants *3*, 105–126.

[Comsol, 2013] Comsol (2013). COMSOL Multiphysics Product Booklet.

[eKlima, 2013] eKlima (2013). Meteorologisk institutt. `http://eklima.met.no` Last checked 05.10.2013.

[Elvevold et al., 2007] Elvevold, S., Dallmann, W. and Blomeier, D. (2007). Geology of Svalbard. Norwegian Polar Institute *1*.

[Førland et al., 2011] Førland, E. J., Benestad, R., Hanssen-Bauer, I., Haugen, J. E. and Skaugen, T. E. (2011). Temperature and Precipitation Development at Svalbard 1900-2100. Advances in Meteorology *2011*, 14.

[Fridleifsson and Freeston, 1994] Fridleifsson, I. B. and Freeston, D. H. (1994). Geothermal energy research and development. Geothermics *23*, 175 – 214.

[Giancoli, 2008] Giancoli, D. (2008). Physics: Principles with Applications with MasteringPhysics. ADDISON WESLEY Publishing Company Incorporated.

[Glassley, 2010] Glassley, W. (2010). Geothermal Energy: Renewable Energy and the Environment. Energy and the Environment, CRC Press.

[Guoyuan et al., 2003] Guoyuan, M., Qinhu, C. and Yi, J. (2003). Experimental investigation of air-source heat pump for cold regions. International Journal of Refrigeration *26*, 12 – 18.

[Haldorsen et al., 1996] Haldorsen, S., Heim, M. and Lauritzen, S.-E. (1996). Subpermafrost Groundwater, Western Svalbard. Nordic Hydrology *27*, 57–68.

[Haldorsen and Lautitzen, 1993] Haldorsen, S. and Lautitzen, S.-E. (1993). Subpermafrost groundwater in Svalbard. Memories of the XXIVth congress of IAH, Ås, Oslo *1*.

[Harris, 1988] Harris, S. (1988). Glossary of Permafrost and Related Ground-ice Terms. Note de service technique / Conseil national de recherches Canada, National Research Council of Canada. Associate Committee on Geotechnical Research.

[Hellström, 2011] Hellström, G. (2011). Borehole heat exchangers. In Geotrainet training manual for designers of shallow geothermal systems pp. 31–53. Geotrainet EFG.

[Hjelle et al., 1999] Hjelle, A., Piepjohn, K., Saalmann, K., Ohta, Y., Salvigsen, O., Thedig, F. and Dallmann, W. (1999). Geological map of Svalbard 1:100,000 Sheet A7G Kongsfjorden. Technical report Norwegian Polar Institute.

[Houghton, 2009] Houghton, J. (2009). Global Warming: The Complete Briefing. Cambridge University Press.

[Huenges and Ledru, 2011] Huenges, E. and Ledru, P. (2011). Geothermal Energy Systems: Exploration, Development, and Utilization. Wiley.

[Humlum et al., 2003] Humlum, O., Instanes, A. and Sollid, J. L. (2003). Permafrost in Svalbard: a review of research history, climatic background and engineering challenges. Polar Research *22*, 191–215.

[Huttrer, 1997] Huttrer, G. W. (1997). Geothermal heat pumps: An increasingly successful technology. Renewable Energy *10*, 481 – 488.

[Isaksen et al., 2001] Isaksen, K., Holmlund, P., Sollid, J. L. and Harris, C. (2001). Three deep Alpine-permafrost boreholes in Svalbard and Scandinavia. Permafrost and Periglacial Processes *12*, 13–25.

[Jørgensen and Bugge, 2009] Jørgensen, P. F. and Bugge, L. (2009). Energiplan Ny-Ålesund. KanEnergi *1*.

[Kristmannsdóttir and Ármannsson, 2003] Kristmannsdóttir, H. and Ármannsson, H. (2003). Environmental aspects of geothermal energy utilization. Geothermics *32*, 451 – 461.

[Liestøl, 1980] Liestøl, O. (1980). Permafrost conditions in Spitsbergen. Frost i jord *21*.

[Lindal, 1973] Lindal, B. (1973). Industrial and other applications of geothermal energy (except power production and district heating). In Geothermal energy; review of research and development Geothermal energy; review of research and development pp. 135–148. UNESCO.

[Lund et al., 2004] Lund, J., Sanner, B., Rybach, L., Curtis, R. and Hellström, G. (2004). Geothermal (ground-source) heat pumps–a world overview. GHC Bulletin *25*, 1–10.

[Lund et al., 2011] Lund, J. W., Freeston, D. H. and Boyd, T. L. (2011). Direct utilization of geothermal energy 2010 worldwide review. Geothermics *40*, 159 – 180.

[Lutgens et al., 2009] Lutgens, F., Tarbuck, E. and Tasa, D. (2009). Essentials of Geology. Pearson Prentice Hall.

[Marshall and Plumb, 2007] Marshall, J. and Plumb, R. (2007). Atmosphere, Ocean and Climate Dynamics: An Introductory Text. International Geophysics, Elsevier Science.

[Midttømme et al., 2008] Midttømme, K., Banks, D., Ramstad, R., Sæther, O. and Skarphagen, H. (2008). Ground-Source Heat Pumps and Underground Thermal Energy Storage— Energy for the future. Geology for Society, Geological Survey of Norway Special Publication *11*, 93–98.

[Midttømme et al., 2010] Midttømme, K., Berre, I., Hauge, A., Musæus, T. and Kristjànsson, B. (2010). Geothermal Energy - Country Update for Norway. Proceedings World Geothermal Congress 2010 .

[Midttømme et al., 2013] Midttømme, K., Nalân, K., Birkelund, Y., Øiseth, O., Braathen, A., Erikson, M. and Oie, V. (2013). Geotermisk energi for Svalbard. `http://cger.no/doc//Kirsti%20Midttomme%20Svalbard.pdf` Last checked 14.11.2013.

[Munson et al., 2006] Munson, B. R., Young, D. F. and Okiishi, T. H. (2006). Fundamentals of fluid mechanics. John Wiley and Sons, Inc.

[Øiseth, 2012] Øiseth, O. (2012). Årsrapport 2012 Kings Bay A/S. http://kingsbay.no/wu07pbtmp/kings_bay_as/annual_reports_2/content/filelist_62e92dd3-e67d-4ab8-82a7-d4d2c40c1b9b/1372593567822/kb_samlet.pdf Last checked 11.12.2013.

[Omer, 2008] Omer, A. M. (2008). Ground-source heat pumps systems and applications. Renewable and Sustainable Energy Reviews *12*, 344 – 371.

[Ore and Øiseth, 2011] Ore, K. M. and Øiseth, O. (2011). Strategiplan Kings Bay A/S 2012-2015. http://kingsbay.no/wu07pbtmp/kings_bay_as/strategic_plan/content/filelist_a2327e76-f691-4269-8006-37c3746edb1b/1372410686140/strategiplan_kings_bay_as_2012_2015.pdf Last checked 11.12.2013.

[Pahud and Matthey, 2001] Pahud, D. and Matthey, B. (2001). Comparison of the thermal performance of double U-pipe borehole heat exchangers measured in situ. Energy and Buildings *33*, 503 – 507.

[Pollack et al., 1993] Pollack, H. N., Hurter, S. J. and Johnson, J. R. (1993). Heat flow from the Earth's interior: Analysis of the global data set. Reviews of Geophysics *31*, 267–280.

[Ramstad, 2011] Ramstad, R. (2011). Grunnvarme i Norge - Kartlegging av økonomisk potensial. Oppdragsrapport A *1*.

[Rybach, 2003] Rybach, L. (2003). Geothermal energy: sustainability and the environment. Geothermics *32*, 463 – 470.

[Sander et al., 2006] Sander, G., Holst, A. and Shears, J. (2006). Environmental impact assesment of the research activities in Ny-Ålesund 2006. Norwegian Polar Institute, Brief Report Series no. 4 *1*.

[Sanner, 2011] Sanner, B. (2011). Overview of shallow geothermal systems. In Geotrainet training manual for designers of shallow geothermal systems pp. 7–15. Geotrainet EFG.

[Sanner et al., 2011a] Sanner, B., Andersson, O., Eugster, W. J. and Arrizabalaga, I. (2011a). Geotrainet training manual for drillers of shallow geothermal systems. European Geothermal Energy Council.

[Sanner et al., 2011b] Sanner, B., Andersson, O., Eugster, W. J., Hellström, G., Arrizabalaga, I., Banks, D., Urchueguía, J. F., Sikora, P., Norbury, D., Polizu, R. and Hanganu-Cucu, R. (2011b). Geotrainet training manual for designers of shallow geothermal systems. GEOTRAINET, EFG, Brussels 2011.

[Schroeder, 2000] Schroeder, D. (2000). An Introduction to Thermal Physics. Addison Wesley.

[Schubert et al., 2001] Schubert, G., Turcotte, D. and Olson, P. (2001). Mantle Convection in the Earth and Planets 2 Volume Set. Cambridge University Press.

[Shears et al., 1998] Shears, J., Theisen, F., Bjørdal, A. and Norris, S. (1998). Environmental impact assessment, Ny-Ålesund international eci-entific research and monitoring station, Svalbard. Norwegian Polar Institute, Meddelelser no. 157 *1*.

[Sollid et al., 2000] Sollid, J. L., Holmlund, P., Isaksen, K. and Harris, C. (2000). Deep permafrost boreholes in western Svalbard, northern Sweden and southern Norway. Norsk Geografisk Tidsskrift - Norwegian Journal of Geography *54*, 186–191.

[Wegener, 1929] Wegener, A. (1929). Die Entstehung der Kontinente und Ozeane. Friedr. Vieweg & Sohn Akt.-Ges.

[Zhang et al., 2000] Zhang, T., Heginbottom, J. A., Barry, R. G. and Brown, J. (2000). Further statistics on the distribution of permafrost and ground ice in the Northern Hemisphere 1. Polar Geography *24*, 126–131.

Appendix A

COMSOL Multiphysics model

Attached with this thesis is the .mph file containing the model which the simulations are based on. The model is created and simulated by using COMSOL Multiphysics 4.3a version 4.3.1.161. The modules used in the simulations are 'Heat transfer in porous media', 'Non-isothermal pipe flow' and 'Darcy's law'.